Time-resolved spin-orbit effects in hydrogen halides

Antonio Cebreiro Gallardo

Máster en Química Teórica y Modelización Computacional

MÁSTERES
DE LA UAM
2020-2021

Facultad de Ciencias

Universidad Autónoma
de Madrid

excelencia UAM CSIC+ Campus Internacional

UNIVERSIDAD AUTONOMA DE MADRID

European Master in

Theoretical Chemistry and Computational Modelling

Time-resolved spin-orbit effects in hydrogen halides

Antonio Cebreiro Gallardo

Director: Jesús González Vázquez
Codirector: Alicia Palacios Cañas
Departamento de Química, Facultad de Ciencias,
Universidad Autónoma de Madrid

FACULTAD DE CIENCIAS

Master Thesis. Course 2020-2021

Universidad Autónoma de Madrid

Contents

Acknowledgments

I would like to acknowledge my tutors Jesús González Vázquez and Alicia Palacios Cañas, who have guided me throughout the master thesis and have allowed me to get into the world of the investigation, even with all the difficulties we have encountered this year due to the Coronavirus pandemic.

I acknowledge the computational time awarded at the *Centro de Computación Científica* of the Universidad Autónoma de Madrid (CCC-UAM).

Abstract

The main objective of this work is to explore the effect of spin-orbit couplings in laser-induced dissociation processes in three hydrogen halides: HCl, HBr and HI. These hydrogen halides present a significant spin-orbit-induced splitting in the excited states, which significantly affects the fragments after photo-dissociation. The heavier the halide, the strongest the coupling. We evaluate these non-adiabatic effects and examine whether these couplings can be neglected for photo-excitation studies. A time-resolved analysis on the coupled electron-nuclear dynamics that is triggered after ionization with a short pulse is performed.

The methodology employed has required the development of a new spectral method. The dynamical study is carried out by solving the time-dependent Schrödinger equation including both electronic and nuclear degrees of freedom. The molecules are assumed initially in its fundamental state, and are excited after the interaction with a short pulse. The energy bandwidth of a finite pulse creates a molecular wave packet that may involve one ore several excited electronic states. We have employed two different approaches: firstly, a spin-free representation of the molecular states, where the spin-orbit couplings are ignored, and, secondly, a simulation in the adiabatic picture properly accounting for the spin-orbit effects, where wave functions adapted to the symmetry of the system ($C_{\infty v}$) are used, including the spin-orbit effect explicitely.

A complete description of the excitation dynamics of hydrogen halides has been provided; as expected, the heavier halides present a stronger spin-orbit coupling, and as a consequence, a larger population transfer occurs among their states. We have observed different time scales; i.e. for HCl, non-adiabatic couplings induce the population transfer 4-5 femtoseconds after excitation, while for HI these effects are already important within the Franck-Condon region.

Resumen

El objetivo principal de este trabajo es explorar el efecto de los acoplamientos espín-órbita en los procesos de disociación inducidos por láser en tres haluros de hidrógeno: HCl, HBr y HI. Estos haluros de hidrógeno presentan una significativa separación spin-órbita en sus estados excitados, lo que afecta significativamente a los fragmentos producto de la fotodisociación. Cuanto más pesado es el haluro, más fuerte es el acoplamiento. Estos efectos no adiabáticos se evalúan y se examinará si estos acoplamientos pueden ser despreciados en los estudios de fotoexcitación. Se ha realizado un análisis con resolución temporal de la dinámica nuclear-electrónica acoplada provocada tras la ionización con un pulso corto.

La metodología empleada ha requerido el desarrollo de un nuevo método espectral. El estudio dinámico se lleva a cabo resolviendo la ecuación de Schrödinger dependiente del tiempo incluyendo los grados de libertad electrónicos y nucleares. Las moléculas, inicialmente en su estado fundamental, se excitan después de la interacción con un pulso corto. El ancho de banda de energía de un pulso finito crea un paquete de ondas moleculares que puede involucrar uno o varios estados electrónicos excitados. Para conseguir esto hemos trabajado con dos "enfoques" diferentes: en primer lugar, una representación sin espín de los estados moleculares, donde se ignoran los acoplamientos espín-órbita, y, en segundo lugar, una simulación en la imagen adiabática que incluye los efectos espín-órbita, donde las functiones de onda son adaptados a la simetría del sistema ($C_{\infty v}$), incluyendo explícitamente el efecto espín-órbita.

Como resultado se ha proporcionado una descripción completa de la dinámica de excitación de los haluros de hidrógeno; como era de esperar, los haluros más pesados presentan un acoplamiento espín-órbita más fuerte, y como consecuencia se produce entre estos una mayor transferencia de población entre los estados. Hemos observado diferentes escalas de tiempo; es decir, los acoplamientos no adiabáticos del HCl inducen la transferencia de población 4-5 femtosegundos después de la excitación, mientras que en el HI estos efectos son importantes dentro de la región de Franck-Condon.

1 General Introduction: Hydrogen Halide Dynamics

Light induced processes play an essential role in a large number of biological mechanisms. The vast majority of photophysical phenomena requires the study of molecular dynamics associated to excited states[1;2;3]. Natural light spectra reach biological tissues in the range from visible to UV frequencies, which may induce excitation in most molecules, and even ionization. The coupled motion of electrons and nuclei that is triggered under visible/UV radiation involves non-radiative electronic states changes: these processes play an important role and are called electronically **non-adiabatic processes**[4]. These can play an important role in diverse chemical properties: for example, spin-orbit coupling effect usually induces phosphorescence[5].

Hydrogen halides provide a simple display for non-adiabatic dynamics in which spin–orbit interactions play an important role; in fact, spin-orbit coupling effects are usually larger in molecules containing heavy atoms. For this reason, the dynamical process of the photo-dissociation in three different hydrogen halides (HCl, HBr and HI) has been explored, using a full quantum mechanical representation of both electronic and nuclear degrees of freedom. For a time-resolved image, we will represent the evolution of the vibronic (vibrational-electronic) wave packets created after the interaction with an ultrashort UV pulses of relatively low frequencies. These three molecules are known to dissociate upon excitation, because in all of them, only the lowest state, of $^1\Sigma^+$ symmetry, presents vibrationally bound states. Considering the spin-orbit couplings, the products that are found after photo-excitation of an hydrogen halide are:[6] [7]:

$$\begin{aligned} HX\ + h\nu \ &\rightarrow \ H(^2S_{1/2})\ +\ X(^2P_{3/2}) \\ &\rightarrow \ H(^2S_{1/2})\ +\ X^*(^2P_{1/2}) \end{aligned}$$

The field-free electron-nuclear dynamics that follows excitation is largely dictated by the spin-orbit (SO) couplings and can thus led to fragmentation in both open channels. These molecules therefore become a valuable benchmark to investigate non-adiabatic effects using *ab initio* methods in full dimension[8]. Inter-system crossing (ISC) can induce population transfer due to the presence of SO coupling. It usually occurs between states of different multiplicities, but also when no-singlet states are involved due to the presence of different microstates sharing the same multiplicity[9].

In order to obtain an accurate description of these effects, it is necessary to use techniques that go beyond the Born-Oppenheimer approximation, i.e. introducing the coupled electron-nuclear motions. The description of the molecular wave function is achieved within the **Born-Huang approximation**, where the total wave function will be written as a product of a nuclear and an electronic wave function. We will then solve numerically the time-dependent Schrödinger equation, which allows us to extract a time-resolved image of the dynamics of the laser-induced molecular dissociation. In order to gain deep insights on the spin-orbit effects, we will perform simulations where these couplings are included, and compare with the counterpart where these couplings are turned off.

2 Theoretical Introduction

2.1 Quantum Molecular Dynamics

2.1.1 Time Dependent Schrödinger equation

In quantum mechanics the state of a system is represented by a *wave function* ψ. Time evolution of a molecular quantum system follows the time-dependent Schrödinger equation (TDSE), expressed in atomic units (au):

$$i\,\frac{d\,\Psi(\vec{R},\vec{r},t)}{dt} = \hat{\mathrm{H}}(\bar{\mathrm{R}},\bar{\mathrm{r}},t)\cdot\Psi(\bar{\mathrm{R}},\bar{\mathrm{r}},t) \tag{1}$$

where R and r are the nuclei and electronic coordinates and $\hat{\mathrm{H}}$ is the total Hamiltonian of the molecule. TDSE is one of the postulates of quantum mechanics where **total Hamiltonian operator** describes the dynamics of the system. In the following, atomic units are employed through the manuscript, unless otherwise stated. As a starting point, to describe the interaction on a molecule with an external electromagnetic field, the full molecular Hamiltonian $\hat{\mathrm{H}}(\bar{\mathrm{R}},\bar{\mathrm{r}},t)$ can be separated in two terms: the first term $\hat{H}^0$, that describes the field-free wave motion, and the second term $\hat{V}$, with the external perturbation as a Hamiltonian term, i.e. a time-dependent potential:

$$\hat{\mathrm{H}}(\bar{\mathrm{R}},\bar{\mathrm{r}},t) = \hat{\mathrm{H}}^{(0)}(\bar{\mathrm{R}},\bar{\mathrm{r}}) + \hat{\mathrm{H}}^{(1)}(\bar{\mathrm{R}},\bar{\mathrm{r}},t) = \hat{\mathrm{H}}^{(0)}(\bar{\mathrm{R}},\bar{\mathrm{r}}) + \hat{\mathrm{V}}(\bar{\mathrm{R}},\bar{\mathrm{r}},t) \tag{2}$$

where $\hat{\mathrm{V}}(\bar{\mathrm{R}},\bar{\mathrm{r}},t)$ is the laser-molecule interaction potential. The field free Hamiltonian $\hat{\mathrm{H}}^{(0)}(\bar{\mathrm{R}},\bar{\mathrm{r}})$ for a system of M nuclei and N electrons can be written as the sum of the nuclear kinetic energy $\hat{\mathrm{T}}_N$ and the potential energy operator $\hat{\mathrm{V}}_N$ of the nuclei, and the rest of the terms are included in the so-called electronic Hamiltonian $\hat{\mathrm{H}}_{el}(\bar{\mathrm{R}},\bar{\mathrm{r}})$:

$$\begin{gathered}\hat{\mathrm{H}}^{(0)} = \hat{\mathrm{T}}_N + \hat{\mathrm{V}}_N + \hat{\mathrm{H}}_{el} = \ \hat{\mathrm{T}}_N + \hat{\mathrm{V}}_N + \hat{\mathrm{T}}_e + \hat{\mathrm{V}}_e + \hat{\mathrm{V}}_{e-N} = \\ -\frac{1}{2}\sum_{\alpha=1}^{M}\frac{\triangledown_\alpha^2}{m_\alpha} + \sum_{\alpha}^{M}\sum_{\beta<\alpha}^{M}\frac{Z_\alpha Z_\beta}{r_{\alpha\beta}} - \frac{1}{2}\sum_{i=1}^{N}\triangledown_i^2 + \sum_{\alpha}^{M}\sum_{i=1}^{N}\frac{Z_\alpha}{r_{i\alpha}} + \sum_{i}^{N}\sum_{j>i}^{N}\frac{1}{r_{ij}}\end{gathered} \tag{3}$$

where $\triangledown^2$ represents the Laplacian with respect to the coordinates of the particles. Although the Hamiltonian can be separated as a sum of different energy terms, in general the wave function cannot be written as a product of functions that only depend on the electronic or nuclear coordinates or as a function of time. However, in the absence of an external field, $\hat{\mathrm{H}}(\bar{\mathrm{R}},\bar{\mathrm{r}},t) = \hat{\mathrm{H}}^{(0)}(\bar{\mathrm{R}},\bar{\mathrm{r}})$ and the eigenstates of the system can be found by solving the time-independent Schrödinger equation (TISE):

$$\hat{\mathrm{H}}\ \Psi_k(\bar{\mathrm{R}},\bar{\mathrm{r}}) = E_k\ \Psi_k(\bar{\mathrm{R}},\bar{\mathrm{r}}) \tag{4}$$

considering the problem as an eigenvalue problem where $k = 1, 2, 3...$ are solutions of TISE, i.e. the eigenstates. In a stationary state $\Psi_i(\bar{\mathrm{R}}, \bar{\mathrm{r}}, t)$ the only dependence on time is given by its eigenvalue E_k:

$$\Psi_k(\bar{\mathrm{R}}, \bar{\mathrm{r}}, t) = \hat{\mathrm{U}}(t, t_0) \cdot \Psi_k(\bar{\mathrm{R}}, \bar{\mathrm{r}}, t_0) \; \rightarrow \; \Psi_k(\bar{\mathrm{R}}, \bar{\mathrm{r}}, t) = e^{-i \cdot E_k \cdot (t - t_0)} \cdot \Psi_k(\bar{\mathrm{R}}, \bar{\mathrm{r}}, t_0) \tag{5}$$

where t and t_0 are the final and the initial time, respectively, and $\hat{\mathrm{U}}(t, t_0)$ represents the so-called evolution operator. The evolution operator is a unitary operator: $\hat{U}^\dagger \cdot \hat{\mathrm{U}} = 1$. Although the phase of a wave function with a defined energy E_k varies in time, the probability density $|\Psi_i(\bar{\mathrm{R}}, \bar{\mathrm{r}}, t)|^2$ of the stationary states remains constant:

$$|\Psi_i(\bar{\mathrm{R}}, \bar{\mathrm{r}}, t)|^2 = \Psi^* \cdot \Psi = \Psi_k^*(\bar{\mathrm{R}}, \bar{\mathrm{r}}) \cdot e^{+i \cdot E_k \cdot (t - t_0)} \cdot \Psi_k(\bar{\mathrm{R}}, \bar{\mathrm{r}}) \cdot e^{-i \cdot E_k \cdot (t - t_0)} = |\Psi_i(\bar{\mathrm{R}}, \bar{\mathrm{r}})|^2 \tag{6}$$

In order to solve the TDSE (eq. 2), we will expand the time-dependent total wave function $\Psi(R, r, t)$ in a basis set of the eigenstates of $H^{(0)}$, i.e. solving eq. 4 for the Hamiltonian of the isolated molecule given in eq. 3. This method of solving the TDSE using a basis set of eigenvalues is known as the **spectral method**. The time-dependent wave function is then written as:

$$\Psi(\bar{\mathrm{R}}, \bar{\mathrm{r}}, t) = \sum_{k=1}^{\infty} c_k(t) \cdot \Psi_k(\bar{\mathrm{R}}, \bar{\mathrm{r}}) \tag{7}$$

where $\Psi_i(\bar{\mathrm{R}}, \bar{\mathrm{r}})$ are the stationary states. This dynamical description of the field-free Hamiltonian follows the Schrödinger picture formulation of the dynamics, since stationary operators are used and the eigenvectors evolve under the effect of the evolution operator. The expansion in equation 7 is called the *general solution* of the TDSE and it represents the system state at each time t. It is important to remark that this solution assumes three statements:

- all the stationary states of the system $\Psi(\bar{\mathrm{R}}, \bar{\mathrm{r}})$ are known in the absence of an external potential.
- stationary states are orthonormal: $< \psi_j | \psi_i >_r = \delta_{ji}$
- stationary states form a complete basis

In case that an external potential is considered, $V(t)$ in equation 2 it is usually expanded perturbatively. For this reason, it is more useful to use the **interaction picture**, also known as Dirac picture, that is considered as a compromise between Heisenberg and Schrödinger pictures[10]. In the interaction picture both the quantum states Ψ and the operators $\mathcal{O}$ carry time-dependence:

$$\begin{array}{lll} \text{Schrödinger picture} \Rightarrow & |\Psi> = |\Psi\ (t)> & \hat{\mathcal{O}} \neq \hat{\mathcal{O}}\ (t) \\ \text{Heisenberg picture} \Rightarrow & |\Psi> \neq |\Psi\ (t)> & \hat{\mathcal{O}} = \hat{\mathcal{O}}\ (t) \\ \text{Dirac picture} \Rightarrow & |\Psi> = |\Psi\ (t)> & \hat{\mathcal{O}} = \hat{\mathcal{O}}\ (t) \end{array}$$

Dirac wave functions are defined as transformed Schrödinger states, meaning the free part of the Hamiltonian, while Dirac operators are transformed similarly to the Heisenberg operators[11]:

$$\begin{aligned} |\Psi_I\ (t) > &= e^{i\cdot\hat{H}_{0,S}\cdot t}\ |\Psi_S\ (t) > \\ \hat{V}_I\ (t) &= e^{i\cdot\hat{H}_{0,S}\cdot t}\ \hat{V}_I\ e^{-i\cdot\hat{H}_{0,S}} \end{aligned} \tag{8}$$

Ψ_I and Ψ_S are the wave functions in Schrödinger and interaction pictures, $\hat{H}_{0,S}$ is the field-free Hamiltonian and $\hat{V}$ is the interaction term.

2.1.2 Adiabatic picture: Born-Oppenheimer approximation

We describe the molecular eigenstates through the total wave function $\Psi(\overrightarrow{R}, \overrightarrow{r})$, which depends on both the electronic and nuclear coordinates. Because at the electronic time scale the nuclei positions are almost constant, the electronic structure can be retrieved independently for each specific nuclear configuration, i.e. using assuming the **Born-Oppenheimer (BO) approximation**.

Then it is possible to write the total wave function $\Psi(\overrightarrow{R}, \overrightarrow{r})$ as a product of a nuclear wave function $\chi(\bar{\mathrm{R}})$ that depends on the nuclear coordinates, and an electronic wave function $\psi(\bar{\mathrm{R}}, \bar{\mathrm{r}})$ which depends parametrically on the nuclear rearrangements and on the electronic coordinates. The molecular eigenfunctions can then be written as:

$$\Psi(\bar{\mathrm{R}}, \bar{\mathrm{r}}) = \sum_{k=1}^{\infty} \chi_k(\bar{\mathrm{R}}) \cdot \psi_k(\bar{\mathrm{R}}, \bar{\mathrm{r}}) \tag{9}$$

This approach is also called the *technique of separation of variables.* $\psi_k(\bar{\mathrm{R}}, \bar{\mathrm{r}})$ form a complete set of basis electronic functions that can be obtained as solutions of the electronic time-independent Schrödinger equation:

$$\hat{\mathrm{H}}_{el} \cdot \psi(\bar{\mathrm{R}}, \bar{\mathrm{r}}) = E_{el}(\bar{\mathrm{R}}) \cdot \psi(\bar{\mathrm{R}}, \bar{\mathrm{r}}) \tag{10}$$

This equation can be interpreted, as Born and Fock stated[12]: "*A physical system remains in its instantaneous eigenstate if a given perturbation is acting on it slowly enough and if there is a gap between the eigenvalue and the rest of the Hamiltonian's spectrum*". Nevertheless, there are some limitations of BO approximation[13]; firstly, it only considers stationary states, meaning it can be used when there are states with eigenfunctions of the electronic Schrödinger equation, that are called **adiabatic** states $\Psi(\bar{\mathrm{R}}, \bar{\mathrm{r}})$. Moreover, it does not include the effects of degeneracy and it is not valid when the variation of the electronic wave function with the nuclear configuration is not smooth.

2.1.3 Non-adiabatic picture: Born-Huang approximation

Born-Oppenheimer approximation is not suitable for all the systems because it does not take into account the non-adiabatic effects. Because the non-adiabatic behaviour cannot be explained only using the Born-Oppenheimer approximation, in 1951 Born and Huang designed the framework for a more general approach to treat the electron-nuclear coupling[18]. **Born-Huang approximation** can be defined as a "non-adiabatic diagonal correction" to the Born-Oppenheimer approximation.

Non-adiabatic corrections allow nuclei to move in more than one electronic state and allow to include the coupling between the electronic and nuclear wave functions. Born and Huang considered $\Psi^0_{sk}(\bar{\mathrm{R}},\bar{\mathrm{r}})$ as adiabatic basis functions that form a complete basis set with electrons and nuclei. Due to adiabatic functions form a complete set, the exact eigenfunctions $\Psi_k(\bar{\mathrm{R}},\bar{\mathrm{r}})$ must fulfill[13]:

$$\Psi_n(\bar{\mathrm{R}},\bar{\mathrm{r}}) = \sum_{ij} C(ij,n)\cdot\Psi^0_{ij}(\bar{\mathrm{R}},\bar{\mathrm{r}}) = \sum_{ij} C(ij,n)\cdot\chi_{ij}(\bar{\mathrm{R}})\cdot\psi_j(\bar{\mathrm{R}},\bar{\mathrm{r}}) \tag{11}$$

where $\chi_{ij}(\bar{\mathrm{R}})$ and $\psi_j(\bar{\mathrm{R}},\bar{\mathrm{r}})$ are the nuclear and electronic wave functions respectively and coefficients $C(sk;n)$ are the expansion coefficients that can be known by solving matrix diagonalization. Operating $\Psi^0_{ij}(\bar{\mathrm{R}},\bar{\mathrm{r}})$ in Hamiltonian of equation 4 it is obtained:

$$\hat{\mathrm{H}}\ \Psi^0_{ij}(\bar{\mathrm{R}},\bar{\mathrm{r}}) = \chi_{ij}\left(\hat{\mathrm{H}}^0_e\ \psi_j\right) + \psi_j\left(\hat{\mathrm{T}}_n\chi_{ij}\right) - \sum_\alpha\left(\frac{1}{2\ M_\alpha}\right)\left[\chi_{ij}\nabla^2_\alpha\psi_j + 2\nabla_\alpha\psi_j\cdot\nabla_\alpha\chi_{ij}\right] \tag{12}$$

where $\hat{\mathrm{H}}^0_e$ is also known as the "champed nuclei" Hamiltonian. $\nabla^2_\alpha\psi_k$ and $\nabla_\alpha\psi_k$ are the BO approximation corrections. Multiplying equation 12 by an arbitrary function ψ^*_l and integrating over electronic coordinates it is obtained:

$$<\psi_l\mid\hat{\mathrm{H}}\mid\Psi^0_{ij}>=\left[\hat{\mathrm{T}}_n\cdot\delta_{jl} + <\psi_l\mid\hat{\mathrm{H}}^0_e\mid\Psi^0_{ij}>_e\ +u_{lj}\ +2\cdot\omega_{lj}\right]\ \chi_{ij}(\bar{\mathrm{R}}) \tag{13}$$

where:

$$\begin{aligned} u_{lj} &= -\sum_\alpha\left(\frac{1}{2\ M_\alpha}\right) <\psi_l\mid\nabla^2_\alpha\mid\Psi^0_{ij}>_e \\ \omega_{lj} &= -\sum_\alpha\left(\frac{1}{2\ M_\alpha}\right) <\psi_l\mid\nabla_\alpha\mid\Psi^0_{ij}>_e\cdot\nabla_\alpha \end{aligned} \tag{14}$$

This off-diagonal terms are the **non-adiabatic corrections** that are usually included in the non-adiabatic coupling matrix[14]:

$$\Lambda_{lj} = u_{lj} + 2\cdot\omega_{lj} = \sum_\alpha\left(\frac{1}{2\ M_\alpha}\right)\left[<\psi_l\mid\nabla^2_\alpha\mid\psi_j>\ +2\ <\psi_l\mid\nabla_\alpha\mid\psi_j>\nabla_\alpha\right] \tag{15}$$

considering $\tau_{lj} \; =< \psi_l \mid \nabla_\alpha \mid \psi_j >$, then:

$$\Lambda_{lj} = \tau_{lj}^2 + 2 \cdot \tau_{lj} \cdot \nabla_\alpha \tag{16}$$

The Schrödinger equation 4 can be rewritten using matrix notation[15]:

$$\left[\hat{\mathrm{T}}_n \mathbf{1} \; + \boldsymbol{V} - \boldsymbol{\Lambda}\right] \; \chi(\bar{\mathrm{R}}) = \boldsymbol{E} \; \chi(\bar{\mathrm{R}}) \tag{17}$$

where $\hat{\mathrm{T}}_n$ is the nuclear kinetic energy, $\boldsymbol{V}$ is the potential energy matrix and $\boldsymbol{\Lambda}$ is the non-adiabatic coupling operators matrix. Due to $\boldsymbol{V}$ is a diagonal matrix that contains the potential energy surfaces calculated with TISE (equation 10), it contains the stationary states eigenvalues.

In the adiabatic picture (BO approx.), the non-adiabatic coupling matrix is not considered, meaning the states are completely decoupled. Although diabatic picture is not really used working with reactants and products, non-adiabatic effects can be really significant working near the transition state, since in general the electronic wave function smoothly changes from reactants to products[16].

If all electronic states were included, equation 16 would be a complete solution to the TDSE. Besides the fact that this solution is very difficult to handle mathematically, states-coupling acts locally in the non-adiabatic regions and only the states the system pass through must be included. The non-adiabatic operator is related to the *derivative coupling vector*, that considering only strongly coupled states it can be expressed as[15]:

$$\hat{\mathrm{F}}_{ij} = \frac{1}{V_j - V_i} \cdot < \psi_i | \frac{\partial \hat{\mathrm{H}}_{el}}{\partial R_\alpha} | \psi_j > \tag{18}$$

It shows the relationship between the derivative coupling and the energy gap $V_j - V_i$ between potential surface between the electronic states. At conical intersections, both potential energy surfaces become degenerate, meaning the coupling is infinite[17]; this is a consequence of the non-adiabatic couplings presence. For this reason, it is more useful to work in the **diabatic picture** where non-adiabatic operator becomes zero by rotation of the previous electronic basis set $\Psi(\bar{\mathrm{R}}, \bar{\mathrm{r}})$ (equation 9) using the unitary transformation U:

$$\Psi_d(\bar{\mathrm{R}}, \bar{\mathrm{r}}) = \boldsymbol{U}(R) \cdot \Psi(\bar{\mathrm{R}}, \bar{\mathrm{r}}) \tag{19}$$

the diabatic nuclear Shrödinger equation becomes:

$$\left[\hat{\mathrm{T}}_n \mathbf{1} \; + \boldsymbol{W}\right] \; \chi_d(\bar{\mathrm{R}}) = \boldsymbol{E} \; \chi_d(\bar{\mathrm{R}}) \tag{20}$$

W is the diabatic potential energy matrix, where coupling terms are included in the off-diagonal matrix potential like terms. Diabatic potential energy matrix can be obtained by an orthogonal transformation of the adiabatic potential energy terms using the same unitary matrix used in equation 19:

$$\boldsymbol{W} = \mathbf{U}^{\dagger} \cdot \boldsymbol{V} \cdot \boldsymbol{U} \tag{21}$$

Both adiabatic and diabatic pictures are related by a unitary transformation; they are related by a rotation of axes in the Hilbert space that does not alter the state vector, i.e. both pictures are equivalent.

2.2 Molecular Structure

2.2.1 Electronic Structure

Due to electron and nuclei motions have been separated using Born-Huang approximation (or Born-Oppenheimer approximation), the diabatic (or adiabatic) energy problem can be considered as an electronic problem where the electronic Schrödinger equation must be solved for each nuclear configuration, obtaining the resulting potential energy surface (PES) that is the basis for solving the nuclear motion. This problem cannot be solved analytically, so that a numerical approach is required and specific approximations, described in the following, are employed.

An independent-particle widely used model is **Hartree-Fock (HF) method**, that considers each electron is described by an orbital; these orbitals are determined by the *variational principle*, meaning they are those with the lowest energy within the restriction of the wave function being a single Slater determinant. Slater Determinant forms the Hilbert space associated to a group of identical fermions (in our case, electrons) and it is consistent with the Pauli and indistinguishability principles:

$$\Psi_0\left(1....N\right) = \frac{1}{(N!)^{\frac{1}{2}}} \begin{pmatrix} \phi_a(1) & \phi_b(1) & ... & \phi_n(1) \\ \phi_a(2) & \phi_b(2) & ... & \phi_n(2) \\ ... & ... & ... & ... \\ \phi_a(N) & \phi_b(N) & .. & \phi_n(N) \end{pmatrix} \tag{22}$$

where N are the number of spin-orbits. The total HF wave function is given as a product of orbitals and it is obtained by minimizing the mean value over the molecular orbital coefficients:

$$E_{HF} = < \psi_{HF} \mid \hat{\mathrm{H}} \mid \psi_{HF} >= min \ < \Psi_0 \mid \hat{\mathrm{H}} \mid \Psi_0 > \tag{23}$$

Hartree-Fock (HF) method it is a iterative method and for this reason it is also denominated self-consistent field method (SCF). It would provide the lowest expectation value to HF energy if the expansion basis set was complete. However, it is necessary to use finite basis sets and the bigger the basis set, the more accurate is the calculation until it is reached the HF limit. This occurs because HF does not include electron correlation (electron–electron interaction is replaced by an average interaction) and it is a mono-configurational method, meaning HF is not a valid method to treat dissociation problems where excited states configurations can be important[20].

One widely used procedure to include several configurations generated by moving electrons from occupied to unoccupied orbitals is the **configuration interaction (CI) method**. In this method, electronic wave function is expanded over a linear combination of Slater determinant that comes from the spin-orbital functions obtained in HF:

$$|\Psi_{CI}> = \hat{\mathrm{A}}\ |\Psi_0> = a_0\ \Phi_{HF} + \sum_{i=1} a_i\ \Phi_i \tag{24}$$

The full CI wave function would include all possible determinants. However, this is computationally not afordable and it is necessary to truncate the number of excited determinants. Although truncation can be performed at single CI (CIS) or single-double CI (CISD) level, with these methods the orbitals would not be optimized and this disadvantage can be avoid by using multi-configurational methods such as the **Multi-Configuration Self-Consistent Field (MCSCF)**. MCSCF is considered as a CI where both the determinants coefficients a_i and the molecular orbital coefficients c_j used for constructing the determinants are optimized:

$$|\Psi_{MC-SCF}>= \hat{\mathrm{C}}\ |\Psi_{CSF}> = \sum_{j=1} c_j\ \Psi_{CSF,j} \tag{25}$$

where $\Psi_{CSF\ j}$ are the configuration state functions, that are related with different Slater determinants included in the expansion. The MCSCF optimization is iterative like the SCF procedure and the most widely used MCSCF method is the **Complete Active Space Self-Consistent Field (CASSCF)** approach. Using CASSCF the selection of the configurations that are necessary to include is done by dividing the molecular orbitals in inactives (doubly occupied), actives (electrons occupancy between 0 and 2) and virtuals (empty). Once the most critical part of orbital selection is done, active orbitals are included in a full CI and the resulting determinants are included in a MCSCF calculation.

In the same way that HF is not able to describe correlation effects, MCSCF is very dependent of the selected active space and can only partially include the correlation energy. Also similar to HF, it is possible to include more correlation by using a configuration interaction, so-called **Multi-Reference Configuration Interaction (MRCI)** method. In this case, excitations are included in a similar fashion than CI but for every configuration included in the CASSCF space.

In the present work, the electronic structure calculations are carried out at the MRCI level, using ANO-RCC basis set (atomic natural orbital-relativistic core-correlated) and as a reference function a CASSCF (6,4) active space, as implemented in the MOLPRO package (computational details are provided in section 3).

2.2.2 Vibrational Structure: B-splines basis set

Assuming the validity of BO approximation, total wave function on bound states (where nuclear repulsion term $\frac{1}{R_{ij}}$ is extracted from Hamiltonian) can be written as:

$$\Psi_{i,v}(\bar{\mathrm{R}},\bar{\mathrm{r}}) = \frac{1}{R}\,\chi_v(\bar{\mathrm{R}})\;\psi_i(\bar{\mathrm{R}},\bar{\mathrm{r}}) \tag{26}$$

where χ_v and $\psi_i(\bar{\mathrm{R}},\bar{\mathrm{r}})$ correspond to the nuclear and electronic wave function in respectively; in this case, the nuclear part corresponds to the vibrational wave function. It has been explained previously that they can be solved by using equations 27 and 28[22]:

$$[H_{el} - E_i\ (R)]\,\psi_i(\bar{\mathrm{R}},\bar{\mathrm{r}}) = 0 \tag{27}$$

$$\left[-\frac{1}{2\mu}\nabla_R^2 + \frac{J(J+1)}{2\mu R^2} + E_i\ (R) - W_{i,v}\right]\chi_v(\bar{\mathrm{R}}) = 0 \tag{28}$$

where $W_{i,v}$ is the total energy of the molecule, E_i the BO potential energy of the i electronic state and J is the total angular momentum.

Molecular dissociation implies the existence of a continuum of vibrational states, non-bound states. The description of a continuum state by using finite coordinates requires a scattering formalism that allows to connect the behaviour of the wave function at long distances with the definition of the function in a finite range of space. In other words, for a numerical treatment of the wave function $\chi_v(\bar{\mathrm{R}})$ the continuum states are replaced by a discretized set of states. For the representation of wave functions that extend over a large range of space, the use of Gaussian or Slater type orbitals, as those employed for bound states, are not longer appropriate. A widely employed alternative is the use of B-spline functions, expanding the vibrational wave function as:

$$\chi_v(\bar{\mathrm{R}}) = \sum_j d_{v,j}\ B_j^k(\bar{\mathrm{R}}) \tag{29}$$

B-spline functions are polynomials of a given degree with conventional properties that make them accurate basis sets in the continuum states description. Three of their main advantages are its ability to diagonalize matrixes even when the banded structure is lost, the flexibility to choose the radial grid points (B-spline basis sets are centred not only in the nucleus, but also in different r) and the ability to use standard Gaussian integrations to evaluate integrals involving B-splines[23]. A well documented review on the use of B-spline functions for the description of continuum functions can be found in Cormier *et. al.* "Applications of B-Splines in Atomic and Molecular Physics"[24].

The use of B-spline basis set in the nuclear Schrödinger equation to describe continuum states is a discretization technique, meaning it encloses the system in a finite interval [0,R] or, in three-dimensions, in a finite box with a certain length R. The lowest eigenvalues from equation 28 diagonalization represent the bound electronic states, and since the basis set is discretized and non-bound continuum states can be normalized to a Dirac delta function:

$$< \psi_i \mid \psi_i >= \delta_{ij} \rightarrow \text{Discrete states}$$
$$< \psi_E \mid \psi_{E'} >= \delta\left(E - E'\right) \rightarrow \text{Continuum states}$$

With Hamiltonian expanded in B-splines basis set, discretized ψ_i and continuum wave functions ψ_{E_i} are related by the density of states ρ, which acts as a normalization factor.

$$\begin{aligned} \psi_{E_i} &= \left|\frac{\partial E(n')}{\partial n'}\right|_{n=n'}^{-\frac{1}{2}} \psi_i \\ \rho(E_n) &= \left|\frac{\partial E(n')}{\partial n'}\right|_{n=n'}^{-1} \end{aligned} \tag{30}$$

being n the index of a given state[24].

2.3 Spin-orbit coupling

2.3.1 Spin-orbit effect description

The Schrödinger treatment is enough for dealing with lightest elements, but heavy elements requires a deeper relativistic treatment in order to have an accurate description of their molecular electronic states. Relativistic effects can remarkably affect chemistry reactions[25;26]; one of the most important effects is the spin-orbit coupling.

Spin-orbit coupling is a relativistic effect defined as the interaction between the spin angular momentum of a particle with its movement in presence of an electrical field. Electron spins interact in atoms by means of the intra-atomic exchange interaction to produce atomic magnetic moments that can drastically change atomic wave functions. The maximum coupling between spin-angular momentum and the electric field occurs when components are perpendicular to each other. The spin-orbit term can be determined from solution of electron state in relativistic case.

The relationship between relativity and quantum mechanics was achieved by P.A.M. Dirac[27], and the most accurate methodology for treating relativistic effects in molecular systems is through the Dirac-Coulomb-Breit equation. Nevertheless, Dirac equation containing four-component "spinors" demands hard computational efforts to be solved (see Bade *et. al.* review[28]) . Thus, there are several quasi-relativistic approximations depending on the problem considered to include the spin-orbit effects. In this work, the approximation that is going to be used is the Douglas-Kroll Hamiltonian.

2.3.2 Spin-orbit operator: Douglas-Kroll Hamiltonian

Due to Dirac-Coulomb-Breit equation solution can be complex and computationally expensive, there are two main alternatives Hamiltonian to calculate the spin-orbit coupling: the Breit-Pauli (BP) and the Douglas-Kroll Hamiltonian. The Breit-Pauli (BP) Hamiltonian, expressed in equation 31[29], is a two-component Hamiltonian. Breit–Pauli (BP) spin–orbit Hamiltonian was presented by Pauli and it is a two-component Hamiltonian obtained by applying a particular unitary transformation (Foldy-Wouthuysen transformation) on the Dirac Hamiltonian[30].

$$\hat{\mathrm{H}}^{BP} = \hat{\mathrm{H}}^{BP}_{SF} + \hat{\mathrm{H}}^{BP}_{SO} + \hat{\mathrm{H}}^{BP}_{MF} \tag{31}$$

The three terms can be computed independently. Firstly, $\hat{\mathrm{H}}^{BP}_{SF}$ refers to the one-body part, it is known as Pauli Hamiltonian and it contains the non-relativistic terms, meaning the **spin-free operators**, that contains the kinetic energy and electron-nuclei potential:

$$\hat{\mathrm{H}}^{BP}_{SF} = \hat{\mathrm{T}} + \hat{\mathrm{V}}_{e-n} \tag{32}$$

The one-body **spin–orbit coupling term** $\hat{\mathrm{H}}^{BP}_{SO}$ of the BP Hamiltonian is[31]:

$$\hat{\mathrm{H}}^{BP}_{SO} = \frac{1}{2\,c^2}\left[\sum_i \left(\sum_l \frac{Z_l}{r^3_{il}}\,(\boldsymbol{r_{il}} \times \boldsymbol{p_i})\right)\cdot \boldsymbol{s}(i) - \sum_{i \neq j} \frac{1}{r^3_{ij}}\,(\boldsymbol{r_{ij}} \times \boldsymbol{p_i}) \cdot (\boldsymbol{s}(i) + 2\boldsymbol{s}(j))\right] \tag{33}$$

where c is the speed of light, Z_l is the nuclei atomic charges, p_i and r_{ij} are the momentum and coordinates and $\boldsymbol{r_{ij}}$ and $\boldsymbol{r_{il}}$ are the electron relative coordinates of the i-th electron. The two-body terms $\hat{\mathrm{H}}^{BP}_{MF}$ includes the spin-spin dipole interactions. Although Breit-Pauli SOC Hamiltonian $\hat{\mathrm{H}}^{BP}_{SO}$ can give accurate results for lower atomic weight species (such as fluorine and chlorine), the results usually deteriorate with the increase of the atomic molecular weight (see Mussard results[29]). This occurs due to the fact that Breit-Pauli SOC is unbounded and overestimates the energy splittings of a heavy atom in a variational calculation. For this reason it is necessary to use a variational stable and non-perturbative Hamiltonian in order to evaluate various energy values and one-electron properties: a good example is the Hamiltonian obtained with Douglas-Kroll approach.

Douglas-Kroll (DK) approach begins with block-diagonalization of the Dirac Hamiltonian $\hat{\mathrm{H}}_D$ removing the off-diagonal elements with a unitary operator (working in two-components)[32]:

$$\boldsymbol{U}\ \hat{\mathrm{H}}_D\ \mathbf{U}^{\mathsf{T}} = \begin{pmatrix} H_+ & 0 \\ 0 & H_- \end{pmatrix} \tag{34}$$

H_+ and H_- are the eigenvalues for the electronic solution of Dirac equation and can be calculated such as an eigenvalue problem (same as TISE). The main goal of Douglas and Kroll procedure is to decompose the unitary transformation $\boldsymbol{U}$ into simpler unitary transformations: free particle matrix, first order DK matrix ... To obtain a deeper demonstration of this procedure see Nakajima,T *The Douglas–Kroll–Hess Approach*.

In regards to this work, the final two-component Douglas–Kroll Hamiltonian can be separated into its spin-free and spin-dependent parts. Using the no-pair approximation[33], where only in the one-electron potential is transformed using DK transformation and the two-electron term is kept in the free-particle, DK Transformed Spin–Orbit coupling Hamiltonian is obtained[32]:

$$\hat{\mathrm{H}}_{DK}^{SO} = \sum_i \sum_l A_i K_i \,\frac{Z_A}{r_{iA}^3}\, (\boldsymbol{r}_{iA} \times \boldsymbol{p}_i) \cdot \boldsymbol{\sigma} A_i K_i - \sum_{i \neq j} A_i K_i A_j \left(\frac{\boldsymbol{r}_{ij}}{r_{ij}^3} \times \boldsymbol{p}_i \right) \cdot (\boldsymbol{\sigma}_i \ + 2\boldsymbol{\sigma}_j)\, A_i K_i A_j \tag{35}$$

where K_i and A_i operators are defined by:

$$\begin{aligned} A_i &= \left(\frac{E_i \ + c^2}{2E_i} \right)^2 \\ K_i &= E_i \ + c^2 \\ E_i &= \left(p^2\ c^2 \ + c^4\right)^2 \end{aligned} \tag{36}$$

where. In the limit $p \to 0$, the spin–orbit Hamiltonian in no-pair approximation goes over to Breit–Pauli SOC Hamiltonian[34]. With this treatment, the spin-orbit Hamiltonian includes both one-electron and two-electrons terms, each treated in a different manner. In heavy elements, the one-electron terms of the spin-orbit Hamiltonians are the dominating parts.

2.3.3 Spin-orbit using spin-free basis

Spin-orbit coupling effect induces coupling of orbital and spin angular momenta; when spin-orbit terms are included in the Hamiltonian, neither spatial symmetry operators nor spin angular momentum operators commute with the Hamiltonian. This problem can be avoid by the using of Wigner-Eckhart theorem, which states that an operator expanded in angular momentum eigenstates basis can be expressed as a product of an independent-angular-momentum orientation part and Clebsch–Gordan coefficients. With this theorem, spin-orbit Hamiltonian elements H_{ij}^{SO} take values different from zero when both states ψ_i and ψ_j direct product of the irreducible representations of the spatial and spin function is equal.

The problem now is how to apply the spin-orbit Hamiltonian. With the electronic eigenvalue problem solved, CASSCF wave functions obtained are "spin-less": spin S affects the electrons permutation symmetry but there is no projection spin M_S, meaning wave functions are eigenstates of S_z but they are a "mix" of all possible spin states within the given multiplet. For this reason, due to electronic spin-free wave functions are invariant to spin rotations, they form a suitable basis for computing spin-orbit matrix elements[35]. Spin-orbit couplings can be studied in a basis formed by eigenstates of the spin-free Hamiltonian:

$$\Psi^{SO} = \sum_{i,\nu_i} c_{i,\nu_i} \, \Psi^{SF}_{i,\nu_i} \tag{37}$$

Spin-free wave function is the reference state and spin-orbit couplings are added as perturbations between states of different spin projection M_S. The presence of projection M_S leads to the presence of **double-group irreducible representations**, that are irreps of a group that double the order of the point group under consideration (due to not only S but also M_s is considered). Forming linear combinations of spin-free wave functions according to the double-groups irreps, the **Hamiltonian is block-diagonalized**. In summary, the spin-orbit state interaction method used in this work consists of the following steps, that are widely described by Meitei *et. al.*[36]:

- Compute the eigenstates of spin-free Hamiltonian
- Compute the spin-orbit matrix elements between all the spin-free states.
- Obtain the total Hamiltonian as a sum of the spin-free and the spin-orbit part.
- Diagonalize the total Hamiltonian

Using these spin-free eigenstates as a basis, it is possible to compute spin-orbit interaction matrix elements, diagonalize the resulting matrix and compute matrix elements over the resulting set of spin-orbit eigenstates.

2.4 Wave packets Dynamics

2.4.1 Laser-molecule interaction: dipole approximation

For the representation of the light-matter interaction term (V(t) in eq. 2), we employ a semi-classical approach, where the electronic (and vibrational) structure is treated quantum mechanically while the electromagnetic field is described classically; i.e. the field it is not quantized, which is known to be a good approximation as long as the light sources under consideration are assumed to present a large flux of photons. This is therefore appropriate to describe the interaction of molecules with ultrashort light pulses as those under consideration. Due to this work is based on the diatomic molecule dissociation and assuming the field only interacts with molecular dipole, perturbation $V(t)$ can be expressed as:

$$\hat{V}(t) = -\bar{\boldsymbol{E}}(\boldsymbol{t}) \cdot \bar{\boldsymbol{\mu}} \tag{38}$$

where $\boldsymbol{\mu}$ is the dipole moment and $\boldsymbol{E}(t)$ is the electric field. Semiclassical dynamic treatment can be applied because the laser radiation makes the number of photons be considered a continuum variable and the properties of the electromagnetic field can be described by *Maxwell equations.* The fields $\mathcal{B}$ and $\mathcal{E}$ can be expressed in terms of a scalar potential $E(\bar{\mathrm{R}}, t)$ and a vector potential $A(\bar{\mathrm{R}}, t)$[37]:

$$\begin{aligned} \mathcal{B}(\bar{\mathrm{R}}, t) &= \nabla \times A(\bar{\mathrm{R}}, t) \\ \mathcal{E} &= -\frac{\partial A}{\partial t} - \nabla \cdot E(\bar{\mathrm{R}}, t) \end{aligned} \tag{39}$$

this two equations describe both the magnetic and the electric fields of an electromagnetic wave. However, there are many different scalar and vector potentials which can generate the same physical electromagnetic field by changing both A and ϕ choosing a gauge transformation for both potentials; in fact, the use of evolution operator in equation 5 is another use of gauge transformation. Now the main question is the correct selection of the gauge transformation in this mathematical procedure.

The evolution of a particle that suffers a Coulombic potential V and laser field with vector potential A and an electrostatic potential E follows the TDSE by the semiclassical Hamiltonian in equation 40[39].

$$H(x, p, t) = \frac{1}{2}\left[p - qA(\bar{\mathrm{R}}, t)\right]^2 + E(\bar{\mathrm{R}}, t) + V(\bar{\mathrm{R}}) \tag{40}$$

For a transversal wave, the propagation is perpendicular to the polarization, which corresponds to applying the *Coulomb gauge restriction* $\nabla A = 0$ on the field, meaning the scalar potential E is zero and the wave equations must follow:

$$\nabla^2 A - \frac{1}{c^2}\frac{\partial^2 A}{\partial t^2} = 0 \tag{41}$$

By substitution, it is observed that $A(\bar{\mathrm{R}},t)$ depends on both space and time coordinates such as:

$$A(\bar{\mathrm{R}},t) = \epsilon \cdot A_0 \cdot cos\,(\omega \cdot t - k \cdot r) \tag{42}$$

where ω is the angular frequency, k is the wave vector in propagation direction, A_0 is the vector potential maximum amplitude and ϵ the polarization vector. When high intensity fields lasers are used and their wavelengths are much longer than the atomic scale (a widely common situation in atomic transitions), **dipole approximation** can be applied. The **dipole approximation** method was originally proposed by Purcell and Pennypacker (1973)[38]. In dipole approach, the spatial dependence of the field is neglected because it is spread over all the system and the vector potential $A(\bar{\mathrm{R}},t)$ can be replaced by $A(0,t)$ in the Hamiltonian:

$$A(t) = \epsilon \cdot A_0 \cdot cos\,(\omega t) \tag{43}$$

The vast majority of *ab initio* methods consider the dipole approximation[39]. Describing atoms-radiation interactions it essentially consists of considering the field is located at the nucleus, neglecting the spatial variation of the electromagnetic field. In the present work, we are exploring molecular excitation, working with wavelengths in the range 200-400 nm, therefore, within the validity of the dipole approximation. The specific parameters of the light sources of interest are presented in section 4.3.1.

There are several equivalent descriptions of the light-matter interaction, but two of the most useful that are going to be used are the length and the velocity gauge[40]:

- In velocity gauge, the field is introduced to the field-free Hamiltonian through the gauge transformation $\boldsymbol{p} \to \boldsymbol{p} - q \cdot A$, where q is the particle charge. Hamiltonian and external potential are defined as:

$$\begin{aligned} \hat{\mathrm{H}}_v &= \frac{1}{2}\left[\boldsymbol{p} - qA(t)\right]^2 + \hat{\mathrm{V}}(\bar{\mathrm{R}},t) \\ \hat{\mathrm{V}}(\bar{\mathrm{R}},t) &= A(t) \cdot \boldsymbol{p} \end{aligned} \tag{44}$$

- In length gauge, the one that is going to be used in this work, the field and the field-free Hamiltonian are:

$$\begin{aligned} H_l &= \frac{p^2}{2} + V(\bar{\mathrm{R}}) - r \cdot E(t) \\ \hat{\mathrm{V}}(\bar{\mathrm{R}},t) &= E(t) \cdot \boldsymbol{r} \end{aligned} \tag{45}$$

2.4.2 Mathematical definition of an Ultrashort Laser Pulse

We are exploring the electron dynamics triggered by ultrashort intense (visible-to-near-infrared) laser pulses and extreme-ultraviolet pulses. They can be simulated with different frameworks: solving numerically the TDSE, using time-dependent perturbation theory, strong-field approximation, etc. An ultrashort laser (Light Amplification by Stimulated Emission of Radiation) is understood as an electromagnetic wave ensemble with a finite total duration, usually, in the range of femtoseconds. Ultrashort laser pulses are represented following the logic of equation 42: pulses with an envelope function $F(t)$ and total duration T so that, for a photon energy ω, the interaction potential and its electric field are written as:[41]:

$$\begin{aligned} &\bar{V}(t) = \bar{E}(t) \cdot \bar{\mu} \\ &\text{E(t)} = \begin{cases} E_0 \cdot \epsilon \cdot F(t) \cdot cos\,(\omega t + \delta) & t = [0, T] \\ 0 & t = \text{elsewhere} \end{cases} \end{aligned} \tag{46}$$

where E_0 is the maximum electric field amplitude and ϵ is the polarization vector. The envelope function $F(t)$ is defined to account for the finite duration of the light, i.e. a "pulse of light". Commonly employed functions to define these envelopes, which provide accurate description of the experimental conditions at which these pulses are generated, are Gaussian or cosine (sine) squared functions, since allows one for an adiabatic switching-on and switching-off of the interacting field. In the present work, the envelope function is defined by a sine squared equation 47:

$$F(t) = sin^2\left(\frac{\pi \cdot t}{T}\right) \tag{47}$$

From the numerical point of view, the use of a sine (or cosine) squared simplifies the numerical implementation in contrast with a Gaussian-type function, because the start and end of the pulse goes to strictly zero. Notice, however, that, although the pulse ends at a given time $t = T$, electrons and nuclei are still interacting and the system continues to propagate under the influence of the field-free Hamiltonian H_0. The spectral amplitude of the pulse is obtained by Fourier transforming the electric field:

$$E(\omega) = \int_0^T E(t) \cdot e^{-i\,\omega\,t} \cdot dt \tag{48}$$

2.5 Wave packet description

Because the energy deposited in the system presents a given bandwidth (ultrashort pulses come with a wide energy range of photons), the wave function that describes the system evolution is indeed a superposition of several eigenstates of the molecule, i.e. a wave packet. In general, a **wave packet** is a localized wave that can be expressed in terms of other properties that are delocalized. In our work, it is a set of wave functions that represents the system.

In quantum mechanics it is widely common to work with probability distributions expressed in a wave function. In most cases it is not necessary to solve the TDSE, since all the information about the dynamics of the system is contained in the time evolution operator; for this reason, the way to work is to *propagate* on time a certain wave function. Working within the *dipole approximation*, and considering the spin-orbit couplings, the total Hamiltonian $\hat{H}(t)$ is written in terms of the total field free Hamiltonian H^0 and the external potential $\hat{V}(t)$ as:

$$\hat{H}^0(\bar{\mathrm{R}},\bar{\mathrm{r}}) = \hat{T}_N(\bar{\mathrm{R}}) + \hat{V}_{el}(\bar{\mathrm{R}},\bar{\mathrm{r}}) - \hat{\Lambda}(\bar{\mathrm{R}},\bar{\mathrm{r}}) + \hat{H}^{DK}_{SO}(\bar{\mathrm{R}},\bar{\mathrm{r}}) \tag{49}$$

$$\hat{\mathrm{V}}(t) = \hat{E}(t)\cdot\bar{\mu} \tag{50}$$

$\hat{\mathrm{V}}_{el}$ is the electronic potential term and $\hat{\mathrm{V}}(t)$ is the external potential applied. Time-dependent Schrödinger equation (eq. 1) can be rewritten using these terms:

$$i\,\frac{d\,\Psi(\vec{R},\vec{r},t)}{dt} = \left[\hat{T}_N + \hat{V}_{el} - \hat{\Lambda} + \hat{H}_{SO} + \bar{\mu}\cdot\hat{E}(t)\right]\cdot\Psi(\bar{\mathrm{R}},\bar{\mathrm{r}},t) \tag{51}$$

In order to solve the TDSE it is used an spectral method expanding the wave function in the adiabatic vibronic stationary states basis[42]:

$$|\Phi(\bar{\mathrm{R}},\bar{\mathrm{r}},t)> = \sum_{N}\sum_{\nu_n} C_{N,\nu_n}\;(t)\;\Psi(\bar{\mathrm{R}},\bar{\mathrm{r}})\cdot e^{-i\cdot E_{N,\nu_n}\cdot t} = \sum_{N}\sum_{\nu_n} C_{N,\nu_n}\;(t)\cdot\chi_k(\bar{\mathrm{R}})\cdot\psi_k(\bar{\mathrm{R}},\bar{\mathrm{r}})\cdot e^{-i\cdot E_{N,\nu_n}\cdot t} \tag{52}$$

where n corresponds to the bound electronic state and and ν_n to its bound or dissociative vibrational states, respectively. Inserting this expansion in equation 49 and projecting into stationary vibronic states, it is obtained a set of coupled differential equations (eq. 53), integrated by using Runge-Kutta procedure[43].

$$i\,\frac{\partial c_{j,\nu_j}(t)}{\partial t} = \sum_{\nu_j}\left[\left(\hat{T}_N\right)_{i,\nu_i\to j,\nu_j} + \left(\hat{V}_{el}\right)_{i,\nu_i\to j,\nu_j} - \hat{\Lambda}_{i,\nu_i\to j,\nu_j} + \left(\hat{H}_{SO}\right)_{i,\nu_i\to j,\nu_j} + \bar{\mu}_{i,\nu_i\to j,\nu_j}\cdot\hat{E}(t)\right]\;c_{j,\nu_j}(t) \tag{53}$$

$c_{j,\nu_j}(t)$ are the time evolution coefficients, needed to define the combination of the basis functions that represents the wave packet evolution.

3 Computational Methods

- **MOLPRO 2012 and 2015**

For the determination of the spin-free potential energy curves, the spin-orbit couplings, and the transition and permanent dipole moments, calculations have been performed using the MOLPRO program, a quantum chemistry software of *ab initio* programs for advanced molecular electronic structure calculations[44]. MOLPRO 2015 has been used for HCl, HBr and HI; after the observation of a bug in the calculation of the spin-orbit coupling in the computational centre software, all calculation were repeated using the previous version MOLPRO 2012. Douglas-Kroll Hamiltonian is used and spin-orbit calculations have been performed using the AMFI method.

- **Spin-orbit effects in spin-free symmetry adapted basis**

Spin-free and spin-orbit energies are calculated using time independent Schrödinger equation (TISE), where eigenstates are the stationary states with Hamiltonian eigenvalues E_i:

$$\begin{aligned} \hat{H}^{SF} \cdot \Psi_i^{SF} &= \mathrm{E}_i^{SF} \cdot \Psi_i^{SF} \\ \hat{H} \cdot \Psi_i^{SO} &= \mathrm{E}_i^{SO} \cdot \Psi_i^{SO} \end{aligned} \tag{54}$$

Spin-free eigenvalue problem is easy to solve because energy matrix $\mathbf{E^{SF}}$ is a diagonal matrix with eigenvalues in the diagonal elements. In the case of spin-orbit Hamiltonian, only relativistic codes can calculate directly the adiabatic spin-orbit states. However, this is not usual due to these codes do not have many prepared methods; for example, the DIRAC code[45] do not have states average CASSCF. The main reason to why not solve directly the spin-orbit couplings is that CASSCF expansion must have all the multiplicities and all the spin projections M_S (singlets, triplets, quintuplets ...) , meaning there should be a basis of too many functions.

As we already comment previously in section 2.3.3, a more common approach is to evaluate *a posteriori* the **spin-orbit coupling over a set of spin-free states**, as an external term of the Hamiltonian. Spin-orbit Hamiltonian is splitted in two parts: spin-free Hamiltonian operator $\hat{H}^{SF}$ that is a diagonal matrix, and the Hamiltonian $\hat{H}^{SO}$ that contains the spin-orbit effects and is an zero-diagonal matrix:

$$\hat{H} = \hat{H}^{SF} + \hat{H}^{SO} \tag{55}$$

Spin-free states Ψ^{SF} are defined by their orbital angular momentum Λ and the electronic spin S. They have *spatial symmetry*: couplings only exists between states of the same symmetry and the Hamiltonian is block-diagonal. On the other hand, spin-orbit states Ψ^{SO} are defined by the orbital angular momentum Λ, the spin S and their spin projection M_S. The presence of spin-orbit coupling leads to the spatial symmetry loss (Σ, Π), all the states can have couplings with each other and Hamiltonian matrix is not block-diagonal. This implies a difficulty in the study of the system in spin-orbit states; however, symmetry can be recovered by the use of **spin-free symmetry adapted basis (SA)**.

While dipole operator $\hat{\mu}$ is directional and basis rotation generates a dipole change according to the symmetry of the molecule (what implies the existence of selection rules), Hamiltonian is a totally symmetric operator, meaning it does not depend on symmetry and it values zero between states of the same symmetry. However, spin-free states with S and $M_s \neq 0$ are not symmetry defined: they must be adapted to a defined symmetry basis in order to simplify the problem. Due to spin-orbit Hamiltonian is totally symmetric, in SA basis the coupling between states of different symmetry $\langle\phi(A1)|\hat{H}^{SO}|\phi(B1)\rangle$, for example, gives zero. As a consequence, spin-orbit Hamiltonian is a block-diagonal matrix using a SA basis.

The spin-orbit eigenstates are obtained by the diagonalization of spin-orbit Hamiltonian over a SA basis Ψ^{SA} consisting on all the spin components of wave functions constructed using the spin-free eigenstates. Ψ^{SA} is obtained by taking appropriate linear combinations of SF states according to the double-group symmetry: for example, the first three SA states belong to A1 symmetry. The first SA state $|\phi_1^{SA}\rangle$ comes from ${}^1\Sigma^+$ in SF. The second SA state $|\phi_2^{SA}\rangle$ is a sum combination of ${}^3\Pi$ SF states with $M_S = 1$ and $M_S = -1$. The third SA state $|\phi_3^{SA}\rangle$ is a subtraction combination of ${}^3\Pi$ SF states also with $M_S = 1$ and $M_S = -1$. Three different SF symmetry states are reorganized by their symmetry in C_{2v} point group in order to obtain three A1 states that only can be coupled between them, simplifying the 12x12 matrix into four 3x3 blocks:

$$\langle\phi_i^{SA}|\hat{\mathcal{O}}|\phi_j^{SA}\rangle = \left(\begin{array}{c|c|c|c} A_1 & 0 & 0 & 0 \\ \hline 0 & B_1 & 0 & 0 \\ \hline 0 & 0 & B_2 & 0 \\ \hline 0 & 0 & 0 & A_2 \end{array}\right)$$

$$|\phi_1^{SA}\ (A_1)\rangle = |{}^1A_1\ (M_s = 0)\ \rangle$$

$$|\phi_2^{SA}\ (A_1)\rangle\ = \frac{1}{\sqrt{2}}\ |{}^3B_1\ (M_s = +1)\ \rangle\ +\ \frac{1}{\sqrt{2}}\ |{}^3B_1\ (M_s = -1)\ \rangle$$

$$|\phi_3^{SA}\ (A_1)\rangle\ = \frac{1}{\sqrt{2}}\ |{}^3B_2\ (M_s = +1)\ \rangle\ -\ \frac{1}{\sqrt{2}}\ |{}^3B_2\ (M_s = -1)\ \rangle$$

$$|\phi_4^{SA}\ (B_1)\rangle = |{}^1B_1\ (M_s = 0)\ \rangle$$

$$|\phi_5^{SA}\ (B_1)\rangle\ = \frac{1}{\sqrt{2}}\ |{}^3A_1\ (M_s = +1)\ \rangle\ +\ \frac{1}{\sqrt{2}}\ |{}^3A_1\ (M_s = -1)\ \rangle$$

$$|\phi_6^{SA}\ (B_1)\rangle = |^3B_2\ (M_s = 0)\ \rangle$$

$$|\phi_7^{SA}\ (B_2)\rangle = |^1B_2\ (M_s = 0)\ \rangle$$

$$|\phi_8^{SA}\ (B_2)\rangle\ = \frac{1}{\sqrt{2}}\ |^3A_1\ (M_s = +1)\ \rangle\ -\ \frac{1}{\sqrt{2}}\ |^3A_1\ (M_s = -1)\ \rangle$$

$$|\phi_9^{SA}\ (B_2)\rangle = |^3B_1\ (M_s = 0)\ \rangle$$

$$|\phi_{10}^{SA}\ (A_2)\rangle = |^3A_1\ (M_s = 0)\ \rangle$$

$$|\phi_{11}^{SA}\ (A_2)\rangle\ = \frac{1}{\sqrt{2}}\ |^3B_1\ (M_s = +1)\ \rangle\ -\ \frac{1}{\sqrt{2}}\ |^3B_1\ (M_s = -1)\ \rangle$$

$$|\phi_{12}^{SA}\ (A_2)\rangle\ = \frac{1}{\sqrt{2}}\ |^3B_2\ (M_s = +1)\ \rangle\ +\ \frac{1}{\sqrt{2}}\ |^3B_2\ (M_s = -1)\ \rangle$$

- **Dipoles and Spin-orbit couplings sign change**

Once the spin-free and adiabatic potential energy curves are obtained for electronic and nuclear states, both dipole and spin-orbit operators have to be expanded in vibronic states basis:

$$\hat{\mathcal{O}}_{i,\nu_1\ j,\nu_2} = \int_0^R \chi_{i,\nu_1} \cdot \langle \phi_i | \hat{\mathcal{O}} | \phi_j \rangle \cdot \chi_{j,\nu_2}\ dR$$

where χ_{i,ν_1} and ϕ_i are the nuclear (vibrational) and electronic wave functions, respectively, and $\hat{\mathcal{O}}$ is the considered operator. These integrals are made utilizing the *Gauss-Legendre integration method.* Potential energy matrix diagonalization at each nuclear configuration makes the phase of the wave function unpredictable: it can take positive or negative values. Due to this fact, dipoles $\langle \psi_i | \hat{\mu} | \psi_i \rangle$ and spin-orbit Hamiltonian $\langle \psi_i | \hat{H}_{SO} | \psi_i \rangle$ have discontinuities when ψ_i sign changes. Therefore, it is necessary to consistently fix the wave function to have a certain phase, meaning the discontinuities that occurs in the same nuclear configurations in $\hat{\mu}$ and $\hat{H}_{SO}$ has to be made continuous.

- **Integration methods**

Time-integration of the system of coupled differential equations (equation 53) is carried out using a Runge-Kutta integration method.

- **Projection into spin-orbit eigenstates**

Results obtained must be defined in eigenstates of the system: spin-free symmetry adapted wave functions are not eigenstates of the system, since the matrix have off-diagonal elements with non-zero values. SA wave functions are eigenstates of spin-orbit Hamiltonian blocks. Using propagation in SA basis, non adiabatic effects are not considered. Only spin-orbit effects, that change with vibronic configurations and they are out of the diagonal, are taking into account. Therefore, it is necessary to project out the wave function in a eigenstates basis:

$$\Psi^{SO} = \sum_{i,\nu_i} c_{i,\nu_i} \, \Psi^{SA}_{i,\nu_i}$$

The adiabatic dynamics are obtained projecting into eigenstates of the spin-orbit Hamiltonian, meaning in the adiabatic states.

4 Results and Discussion

4.1 Molecular structure results

MOLPRO package allows us to perform calculations with abelian point groups, meaning those point groups in which internal operation satisfies the commutative property. Hydrogen halides belong to $C_{\infty v}$ point group symmetry, and consequently the electronic structure simulations are retrieved considering a C_{2v} symmetry. The first step is to obtain the reference wave function for the equilibrium geometry of each molecule using SCF procedure. In a second step, multi-configurational CASSCF method is obtained using an (6,4) active space formed by orbital H-1s with A_1 symmetry and three last halogen orbitals p_x, p_y and p_z with B_1, B_2 and A_1 symmetry, respectively, due to bond axis is considered to be in z-direction.

In the third step, CASSCF wave function is used as the reference function to diagonalize the full Hamiltonian and solve the eigenvalue problem within a MR-CI calculation, performed using an ANO-RCC basis set[46] and considering a Douglas-Kroll Hamiltonian to have into account one-electron relativistic effects. In the fourth step, eigenenergies (potential energy for each nuclear configuration), electronic dipoles and the spin-orbit couplings are calculated. potential energy curves are used in eq. 4 for the nuclear eigenvalue problem to extract the vibrational structure, where the wave functions are written in a basis set of B-spline functions.

4.1.1 Electronic Energy Curves for HCl, HBr and HI.

Electronic Hamiltonian operator eigenvalues have been calculated as the solutions of time-independent Schrödinger equation in the basis of spin-free wave functions:

$$< \varphi_i^{SF} \mid \hat{\mathrm{H}}^{SF} \mid \varphi_j^{SF} > = E_i^{SF} \; \delta_{ij} \tag{56}$$

When spin-orbit coupling is not taken into account, the quantum numbers that define the electronic states are Λ, S^2 and Σ. As it can be observed in pictures 1, 2 and 3 there are four adiabatic spin-free electronic states defined by their projection of the orbital angular momentum Λ and their electronic spin Σ: $X\ ^1\Sigma^+$ (non degenerate), $^1\Pi$ (double degenerate), $^3\Pi$ (sixfold degenerate) and $^3\Sigma^+$ (threefold degenerate). Since the spin-orbit is neglected at this stage, all of them correlate to the ground state $H\ ^2S\ + X\ ^2P$, meaning they have the same asymptotic energy value.

The equilibrium internuclear distances obtained with the spin-free simulations are 2.46, 2.65 and 3.02 au for HCl, HBr and HI, respectively. These bond distances are in very good agreement with experimental results compiled by Huber[50] for the three molecules, 2.41, 2.67 and 3.04 au. Total energy at ground state $^1\Sigma^+$ in the equilibrium distances values -461.753 au in HCl, -2605.112 au in HBr and -7111.628 au in HI.

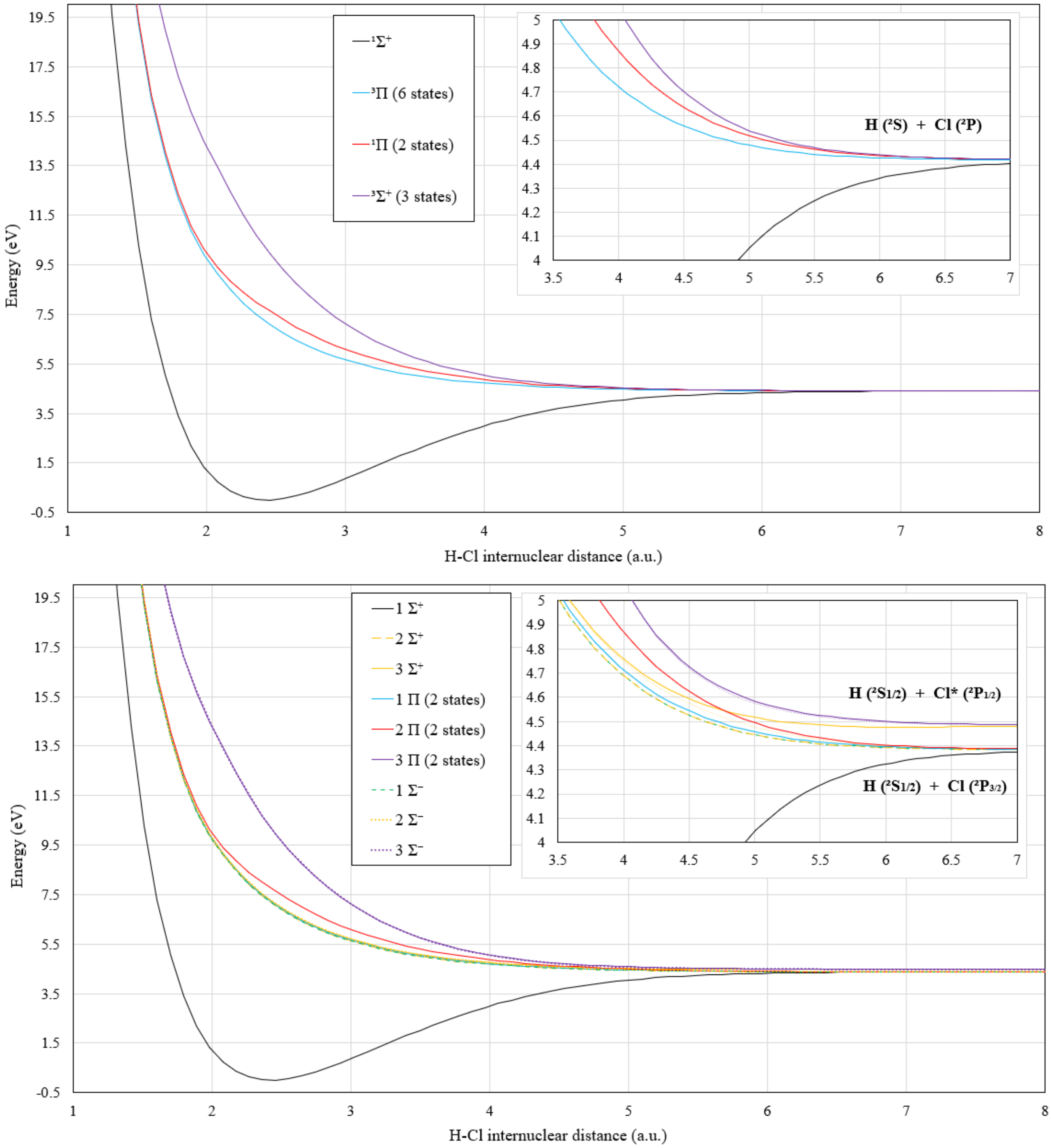

Figure 1: Spin-free (top picture) and adiabatic (bottom picture) electronic potential energy curves of HCl molecule. Energies have been calculated using MRCI method.

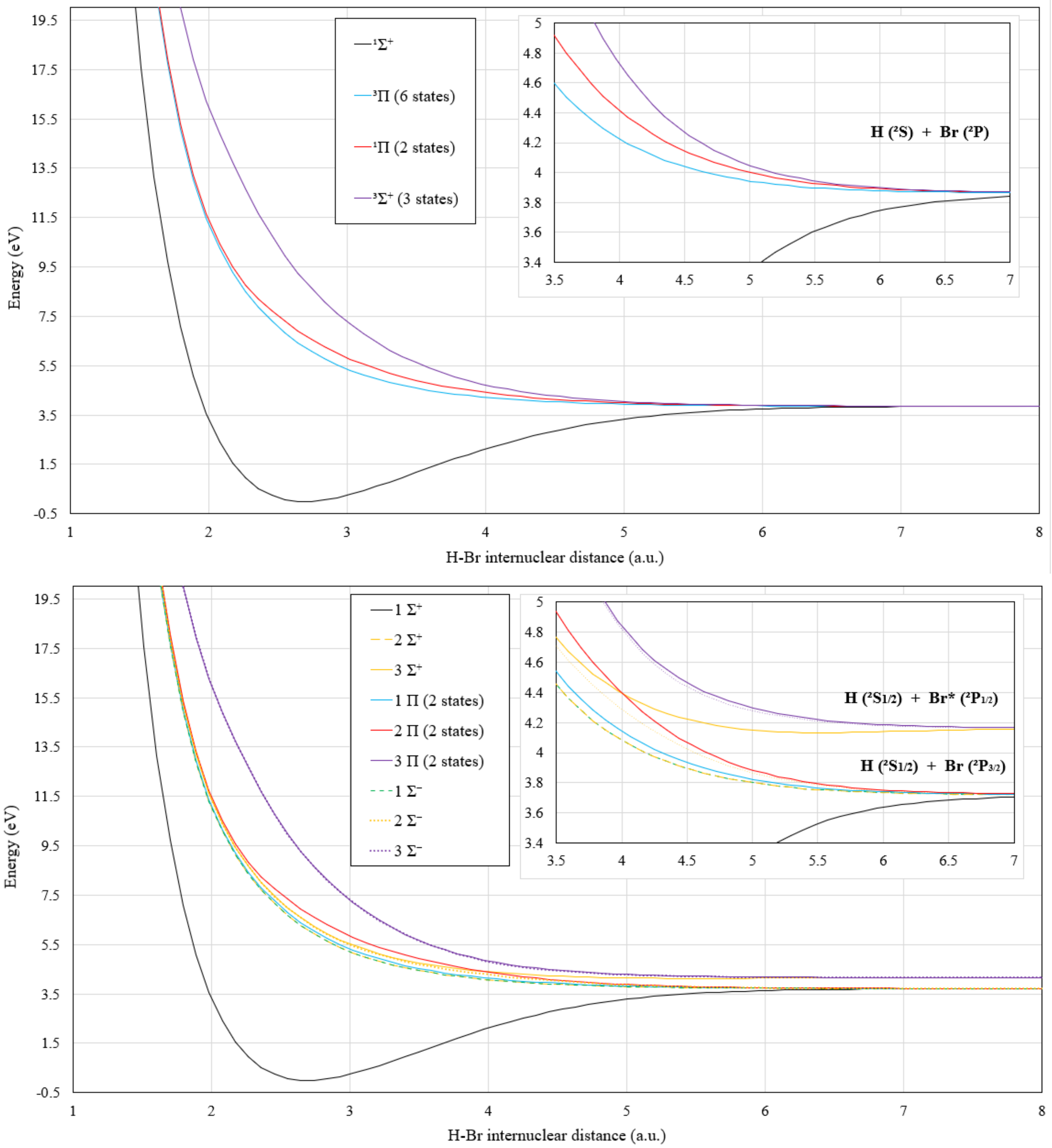

Figure 2: Spin-free (top picture) and adiabatic (bottom picture) electronic potential energy curves of HBr.

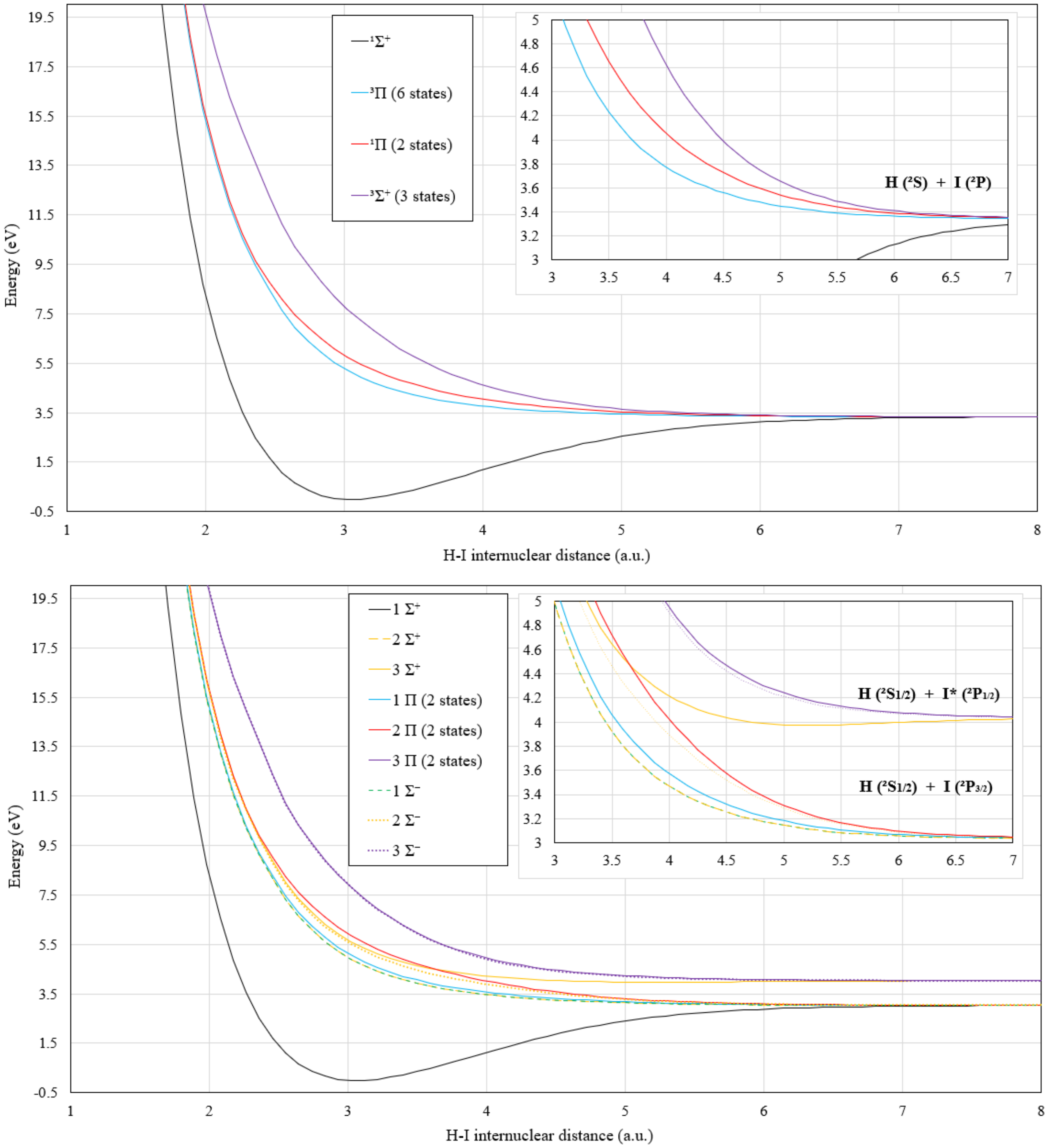

Figure 3: Spin-free (top picture) and adiabatic (bottom picture) electronic potential energy curves of HI.

Once spin-free quantum calculations are obtained, wave functions are projected into the irreducible representations corresponding to arbitrary symmetries in order to generate spin-free symmetry adapted wave functions. Nevertheless, unitary transformation that generates a basis change does not modify the Hamiltonian operator, meaning the potential curves are the same although their order is determined by their symmetry.

When spin-orbit couplings are taken into account, adiabatic states are studied. Adiabatic potential energy curves are calculated by diagonalizing a matrix with spin-free potential energy curves in the diagonal-elements and spin-orbit couplings in off-diagonal elements:

$$< \varphi_i^{SA} \mid \hat{\mathrm{H}}_{el} \mid \varphi_j^{SA} > = E_i^{SA} \, \delta_{ij} + < \varphi_i^{SA} \mid \hat{\mathrm{H}}_{SO} \mid \varphi_j^{SA} > \tag{57}$$

While spin-free potential curves tend to the same asymptotic limit, in adiabatic curves there are two dissociation channels: $H(^2S)\ + X\ (^2P_{\frac{3}{2}})$ and $H(^2S)\ + X^*\ (^2P_{\frac{1}{2}})$. There are eight adiabatic electronic states that correlate to the dissociation fragment $X\ ^2P_{3/2}$: $X\ 1\Sigma^+$, $2\Sigma^+$, 1Π (double degenerate), 2Π (double degenerate), $1\Sigma^-$ and $2\Sigma^-$. The other four adiabatic states $3\Sigma^+$, 3Π (double degenerate) and $3\Sigma^-$ correlate to excited-state $X^*\ ^2P_{1/2}$. Dissociation energies of both dissociation channels also agree with computational references, as it is shown in table 1. The good agreement of these calculated properties with experimental references (shown with each reference value) is evidence of accuracy.

Table 1: Dissociation energies in adiabatic states for both dissociation channels.

	$H(^2S)\ + X\ (^2P_{\frac{3}{2}})$	**Reference Value**	$H(^2S)\ + X^*\ (^2P_{\frac{1}{2}})$	**Reference Value**
HCl	4.388	4.340	4.488	4.567 [47]
HBr	3.727	3.746	4.168	4.096 [48]
HI	3.044	3.054	4.044	3.997 [49]

The energy difference between both adiabatic dissociation channels varies depending on the molecule considered: as expected, the heavier the halogen is, the stronger the spin-orbit is, what is observed in an increase of the energy difference between both dissociation channels. The energy between both asymptotic limits values 0.10 eV in the case of HCl, in HBr this variable values 0.44 eV and in HI it increases until 1.00 eV. Comparing with experimental results, HCl, HBr and HI energy differences between $X\ ^2P_{\frac{3}{2}}$ and $X^*\ ^2P_{\frac{1}{2}}$ are 0.12[51], 0.46[52] and 0.94[53] eV, meaning computational and experimental energies agree.

On the other hand, the distance value at which intersystem crossing occurs decreases when the halogen atom weight increases: it is observed at 4.72 au in HCl, at 3.97 au in HBr and at 3.69 au in HI. As it is going to be explained, the internuclear distance at which this transition between the two adiabatic electronic states $3\ \Sigma^+$ and $2\ \Pi$ is going to strongly modify the wave packet evolution, and consequently, the final fragmentation ratios.

4.1.2 Vibrational Energy curves

Once the electronic structure and the electronic potential energy curves have been obtained for a fine grid and large enough range of internuclear distances, the next step is to obtain of vibrational eigenstates. Vibrational wave functions are expanded using a basis set of 320 8th degree B-spline functions. Eigenstates are obtained by solving the one-dimensional Schrödinger equation in a box of length 13 au length box, shown in equations 28 and 29.

$$\text{Schrödinger vibrational equation } \Rightarrow \left[-\frac{1}{2\mu}\nabla_R^2 + \frac{J(J+1)}{2\mu R^2} + E_i\ (R) - W_{i,v}\right]\chi_v(\bar{\mathrm{R}}) = 0$$

$$\text{B-splines basis expansion } \Rightarrow \chi_v(\bar{\mathrm{R}}) = \sum_j d_{v,j}\ B_j^k(\bar{\mathrm{R}})$$

where μ corresponds to the molecules reduced mass (1786.398, 1814.297 and 1822.706 for HCl, HBr and HI, respectively), $E_i\ (R)$ to the potential energy curve of each i-th electronic state as a function of the internuclear distance R and $W_{i,v}$ are the vibrational states ν associated to the electronic state i.

By the use of B-spline functions continuum states have been discretized; for this reason, the density of each vibrational level has to be considered in the next excitation probabilities and consequently in the wave packet. Figure 4 shows five vibronic eigenstates in the ground state $^1\Sigma^+$ for each molecule, and figure 5 shows five vibronic states for the first excited state $^1\Pi$.

Those vibrational levels with less energy than their electronic state dissociation limit are considered bound vibrational levels, while those with higher energy are considered continuum vibrational states. In all the three molecules there are twenty bound vibrational levels in the ground state, meaning the twenty-first level is the first dissociative one. Figure 4 shows that energy difference between vibronic levels decreases when the halogen atom weight in the molecule increases: for example, energy difference between levels with vibrational quantum number $\nu = 0$ and $\nu = 20$ is 4.24 eV in HCl, 3.72 in HBr and 3.21 eV. This is consistent with the expected progressions in vibronic frequencies, which are inversely dependent on the reduced mass $E_\nu \propto \mu^{-\frac{1}{2}}$.

Zero-point energy values for HCl, HBr and HI are 0.182, 0.156 and 0.141 eV, respectively. These results agree with the computational reference values calculated with CISD method (6-31G* basis set for HCl and HBr, 6-311G* for HI): in HCl takes the value of 0.188, in HBr 0.164 eV and in HI 0.141 eV[54]. While in the ground state there are twenty bound vibronic states, the first excited state $^1\Pi$ have all its vibrational levels above its dissociation limit in all the molecules, as it can be observed in picture 5. Therefore this electronic state does not have any bound state and consequently it is a purely dissociative electronic state.

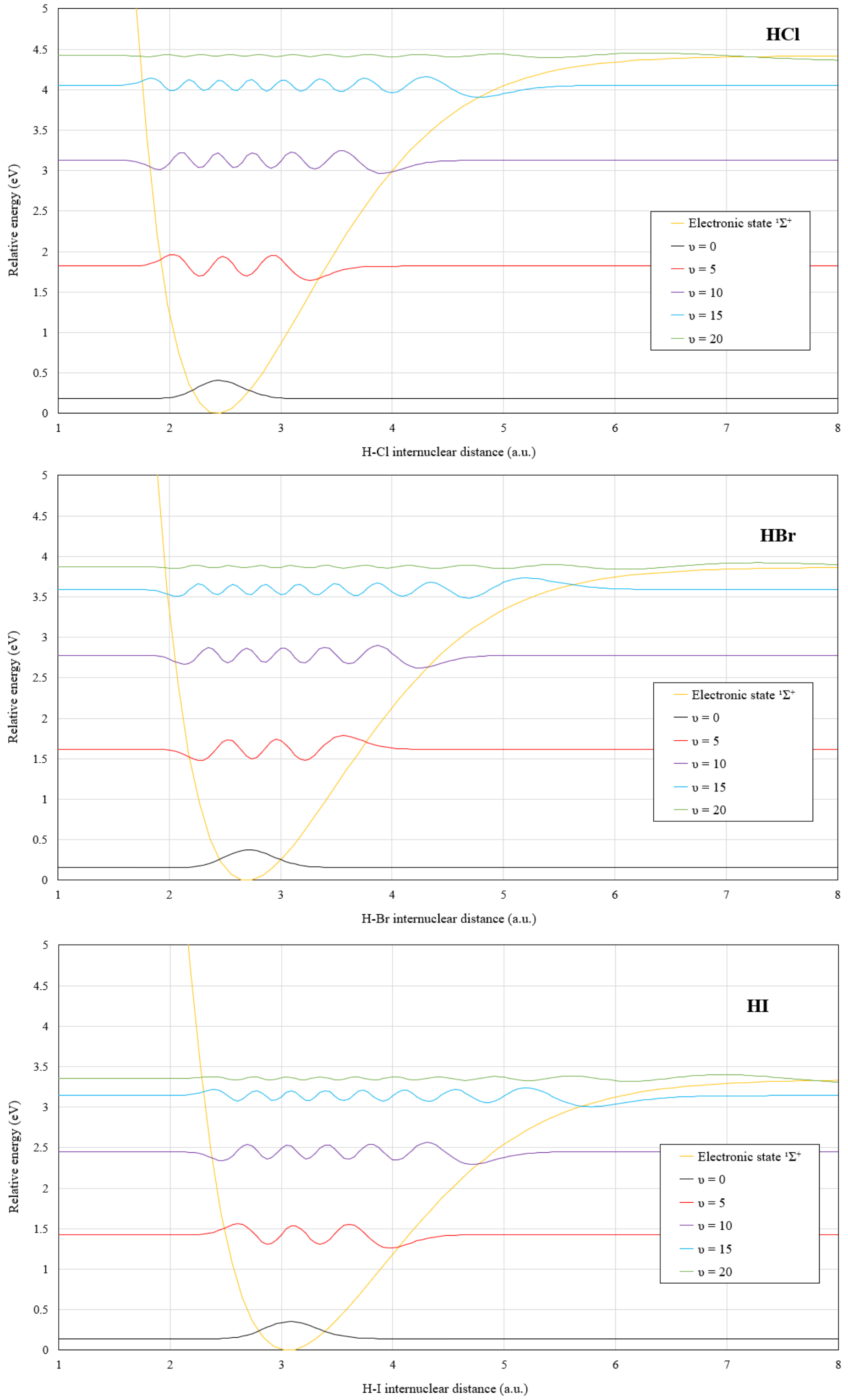

Figure 4: Five different discretized continuum vibrational states of diabatic ground electronic state $^1\Sigma^+$ in HCl (top panel), HBr (middle panel) and HI (bottom panel). These levels have been calculated solving one-dimensional Schrödinger equation in a 13 au length box with B-splines basis set.

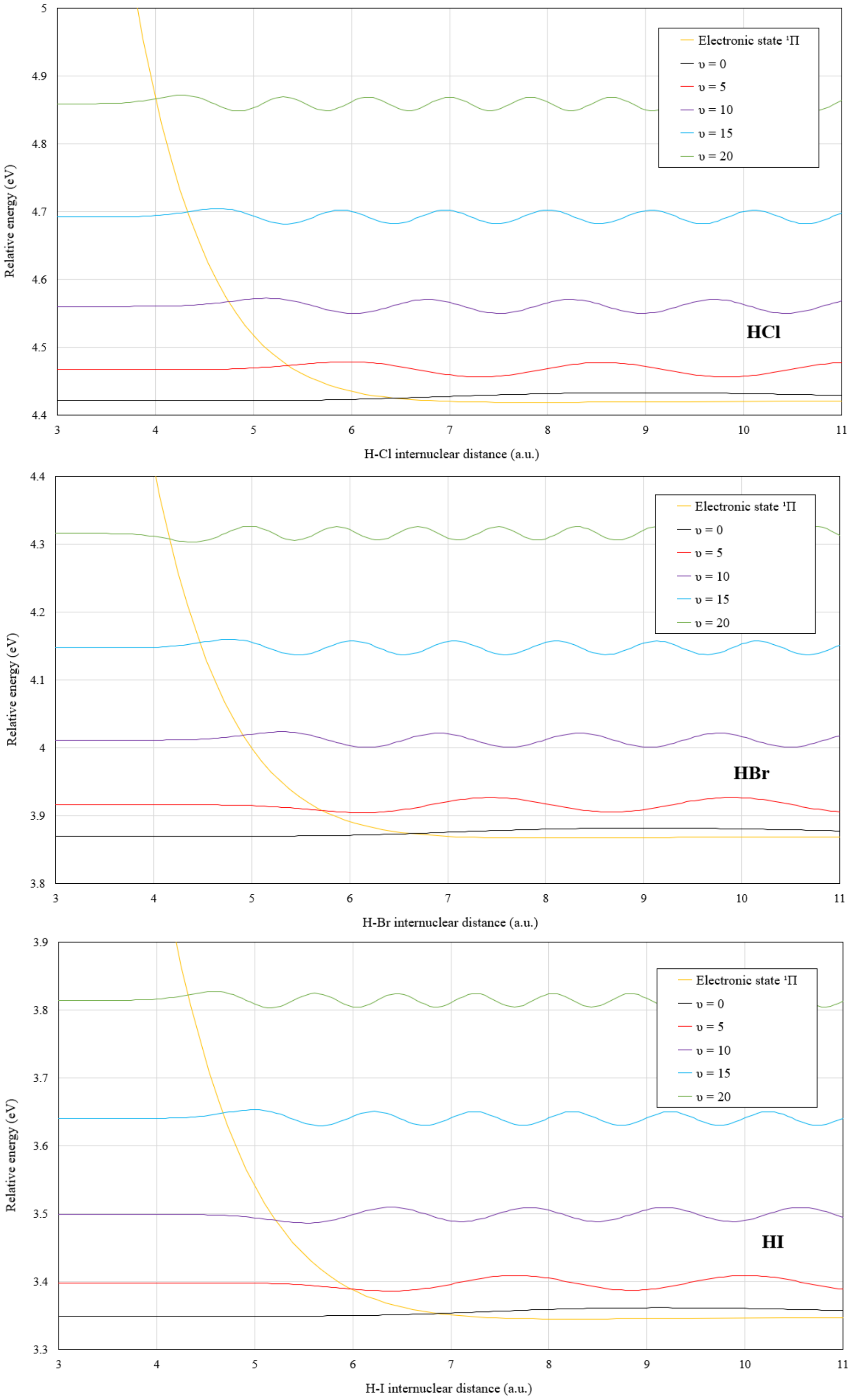

Figure 5: Five different discretized continuum vibrational states of diabatic bound excited electronic state $^1\Pi$ in HCl (top panel), HBr (middle panel) and HI (bottom panel).

4.2 Couplings

Dipoles and spin-orbit couplings between vibronic levels of each electronic states have been calculated and integrated utilizing the Gauss-Legendre integration method.

$$\hat{O}_{i,\nu_1\ j,\nu_2} = \int_0^R \chi_{i,\nu_1} \cdot < \phi_i | \hat{O} | \phi_j > \cdot \chi_{j,\nu_2}\, dR \tag{58}$$

4.2.1 Dipole couplings

Dipole operator can be well understood by the knowledge of each electronic state symmetry. In spin-free basis, symmetry is defined by projection of the orbital angular momentum along the internuclear axis Λ and spin S. Consequently molecular selection rules ($\Delta S = 0$) imply that, in perpendicular direction to molecular axis (x and y-component), only exists dipole coupling μ between electronic ground state $^1\Sigma^+$ and excited state $^1\Pi$. Due to $^1\Pi$ electronic state is doubly degenerated, there are two dipoles of the same magnitude in x and y directions, meaning this state is going to be populated with x and y-polarized laser. On the other hand, in molecular bond axis there is a permanent dipole μ_z of state $^1\Sigma^+$ and itself.

The expansion of adiabatic picture in the spin-free symmetry adapted basis implies the use of C_{2v} point group symmetry, as it has been explained in section 3. Dipole operator μ_x, due to it works in x-direction, acts according to B_1 irreducible representation (irrep): B_1 applied to A_1 irrep operator gives $A_1 \otimes B_1 = B_1$, meaning B_1 and A_1 states are coupled by x-dipole. x-dipole irrep B_1 applied to A_2 states gives $A_2 \otimes B_1 = B_2$, meaning B_2 and A_2 states are coupled by x-dipole. These selection symmetry rules imply that the ground state $1\Sigma^+$ (symmetry A_1) using x-polarized light can only transfer population to B_1 states. These dipole couplings between SA states are schematically written in Table 2.

Table 2: Dipole couplings expanded in SA basis between wave functions of different symmetries.

	$\boldsymbol{A_1}$	$\boldsymbol{B_1}$	$\boldsymbol{B_2}$	$\boldsymbol{A_2}$
$\boldsymbol{A_1}$	μ_z	μ_x	μ_y	0
$\boldsymbol{B_1}$	μ_x	μ_z	0	μ_y
$\boldsymbol{B_2}$	μ_y	0	μ_z	μ_x
$\boldsymbol{A_2}$	0	μ_y	μ_x	μ_z

Figure 6 (spin-free states) and 7 (adiabatic states) shows the transition and permanent dipole couplings as a function of the internuclear distances for HCl, HBr and HI. Left side panels show the couplings for the light polarization vector on the molecular axis (z-direction), while right side panels show the couplings for the light polarization vector perpendicular to the molecular axis (x and y-direction).

Both on spin-free and adiabatic states, it is noticed that the heavier the halogen atom, the larger is the maximum value obtained for the dipole coupling in x,y-direction (left panels) and the more is shifted to larger distances. HCl dipole maximum in spin-free states values 0.73 D (R = 1.04 au), in HBr 0.81 D (R = 1.32 au) and in HI 0.96 D (R = 1.79 au). After the maximum value, $^1\Sigma^+ -^1\Pi$ dipole decreases drastically in all the three molecules, and slope is the highest in HI. Relevant values in a one-photon transition from the ground state are those around the equilibrium internuclear distances (due to dynamics starts in Franck-Condon region) working in perpendicular with respect to the bond axis (x or y-direction): this is 0.22 au in HCl, 0.19 au in HBr and 0.04 au in HI (values marked with a point in fig. 6).

On the other hand, dipole couplings in bond axis (z-direction, right plots in figure 6 and 7), unlike in the x and y directions, decreases its value when the halogen atomic number increases. The permanent dipole μ_{11} does not change in both spin-free and adiabatic picture, but in the adiabatic picture it is also observed the presence of coupling μ_{13} with state $3\Sigma^+$.

HBr adiabatic dipole moment curves are similar to those obtained by Valero *et. al.*[55] and Smolin[48] works, who follow this same procedure. Werner and Rosmus work[56], using SCEP/CEPA (self-consistent electron pair / coupled electron pair) wave functions, show spin-free dipole moments in the vibrational ground states are calculated to be (experimental values in parenthesis) 1.120 D (1.1085 D) for HCI and 0.829 D (0.828 D) for HBr.

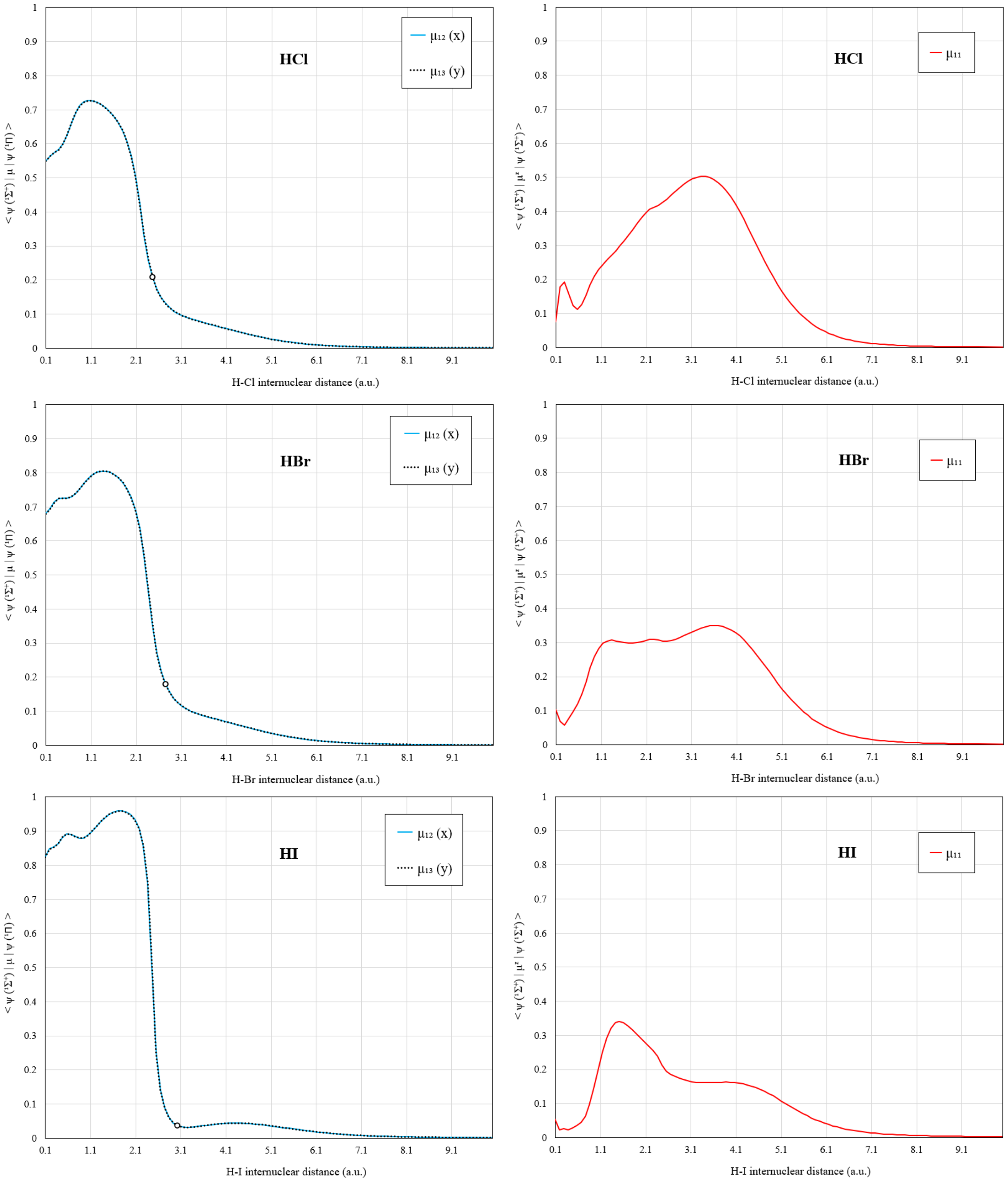

Figure 6: Dipole couplings of spin-free states as a function of the internuclear distances for HCl (top panels), HBr (middle panels) and HI (bottom panels). Left side panels show the couplings for the light polarization vector perpendicular to the molecular axis (from $^1\Sigma^+$ to $^1\Pi$). Right side panels show the couplings for the light polarization vector light polarization vector on the molecular axis (permanent dipole associated to the fundamental state). Empty points indicate the molecular equilibrium distance.

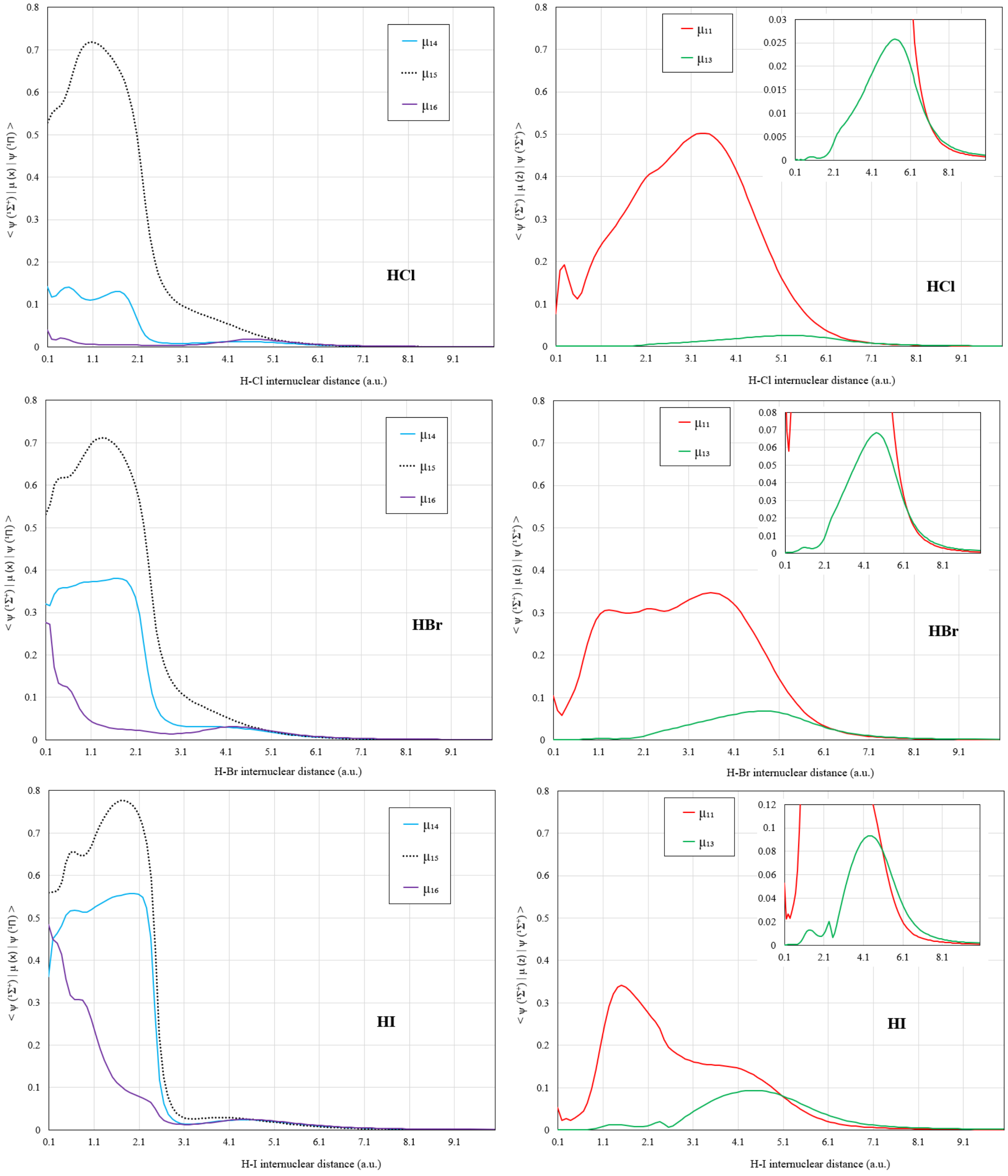

Figure 7: Dipole couplings of adiabatic states as a function of the internuclear distances for HCl (top panels), HBr (middle panels) and HI (bottom panels). Left side panels show the couplings for the light polarization vector perpendicular to the molecular axis (from $1\Sigma^+$ to $1\Pi,2\Pi,3\Pi$). Right side panels show the couplings for the light polarization vector on the molecular axis (permanent dipole associated to the fundamental state and from $1\Sigma^+$ to $3\Sigma^+$).

4.2.2 Spin-orbit couplings

Spin-orbit couplings are expanded in spin-free symmetry adapted basis to rearrange the spin-orbit Hamiltonian matrix by symmetry and only have couplings between states of the same symmetry:

$$\langle\phi_i^{SA}|\hat{\mathcal{H}}^{SO}|\phi_j^{SA}\rangle = \begin{array}{c|cccccccccccc} & 1\Sigma^+ & 2\Sigma^+ & 3\Sigma^+ & 1\Pi & 2\Pi & 3\Pi & 1\Pi & 2\Pi & 3\Pi & 1\Sigma^- & 2\Sigma^- & 3\Sigma^- \\ \hline 1\Sigma^+ & A_1 & A_1 & A_1 & 0 & 0 & 0 & 0 & 0 & 0 & 0 & 0 & 0 \\ 2\Sigma^+ & A_1 & A_1 & A_1 & 0 & 0 & 0 & 0 & 0 & 0 & 0 & 0 & 0 \\ 3\Sigma^+ & A_1 & A_1 & A_1 & 0 & 0 & 0 & 0 & 0 & 0 & 0 & 0 & 0 \\ 1\Pi & 0 & 0 & 0 & B_1 & B_1 & B_1 & 0 & 0 & 0 & 0 & 0 & 0 \\ 2\Pi & 0 & 0 & 0 & B_1 & B_1 & B_1 & 0 & 0 & 0 & 0 & 0 & 0 \\ 3\Pi & 0 & 0 & 0 & B_1 & B_1 & B_1 & 0 & 0 & 0 & 0 & 0 & 0 \\ 1\Pi & 0 & 0 & 0 & 0 & 0 & 0 & B_2 & B_2 & B_2 & 0 & 0 & 0 \\ 2\Pi & 0 & 0 & 0 & 0 & 0 & 0 & B_2 & B_2 & B_2 & 0 & 0 & 0 \\ 3\Pi & 0 & 0 & 0 & 0 & 0 & 0 & B_2 & B_2 & B_2 & 0 & 0 & 0 \\ 1\Sigma^- & 0 & 0 & 0 & 0 & 0 & 0 & 0 & 0 & 0 & A_2 & A_2 & A_2 \\ 2\Sigma^- & 0 & 0 & 0 & 0 & 0 & 0 & 0 & 0 & 0 & A_2 & A_2 & A_2 \\ 3\Sigma^- & 0 & 0 & 0 & 0 & 0 & 0 & 0 & 0 & 0 & A_2 & A_2 & A_2 \end{array}$$

Therefore, for example, ground state $1\Sigma^+$, belonging to A_1 symmetry, only have spin-orbit (SO) couplings with the other two A_1 states. With $2\Sigma^+$ electronic state couples in the real Hamiltonian part and with $3\Sigma^+$ electronic state couples in imaginary Hamiltonian part, so both spin-orbit couplings have the same module and differ by their phase. Figure 8 shows SO couplings module between A_1 states ($1\Sigma^+$ and $2\Sigma^+$) and between B_1 states (1Π and 2Π) for the three molecules.

First of all, in both irreps SO coupling magnitude increases with the atomic number. This fact fits to the Douglas-Kroll Hamiltonian operator that directly depends on atomic number, as it is shown in equation 35. Secondly, the evolution of SO coupling with respect to the distance explains the use of symmetry adapted basis: if these SO couplings and the energy difference between spin-free states were constant with distance, the evolution of the system would occur in adiabatic states (eigenstates of the system). Nevertheless, at shorter distances SO coupling varies; in fact, at equilibrium distance occurs the highest spin-orbit variation. This is the reason why it is difficult to work directly in adiabatic states.

At larger distances from equilibrium, SO coupling keeps a constant value and energy difference between states is also constant, i.e. there cannot exist population transfer between coupled states. At this point, SO atomic value is reached: it values 0.00174, 0.00762 and 0.01729 au for HCl, HBr and HI, respectively. In A_1 states the constant coupling is reached at $R = 2.83$ au in HCl ($R_{eq} = 2.41$ au), at 3.59 au in HBr ($R_{eq} =$ 2.67 au) and at 4.06 au in HI ($R_{eq} = 3.04\ au$).

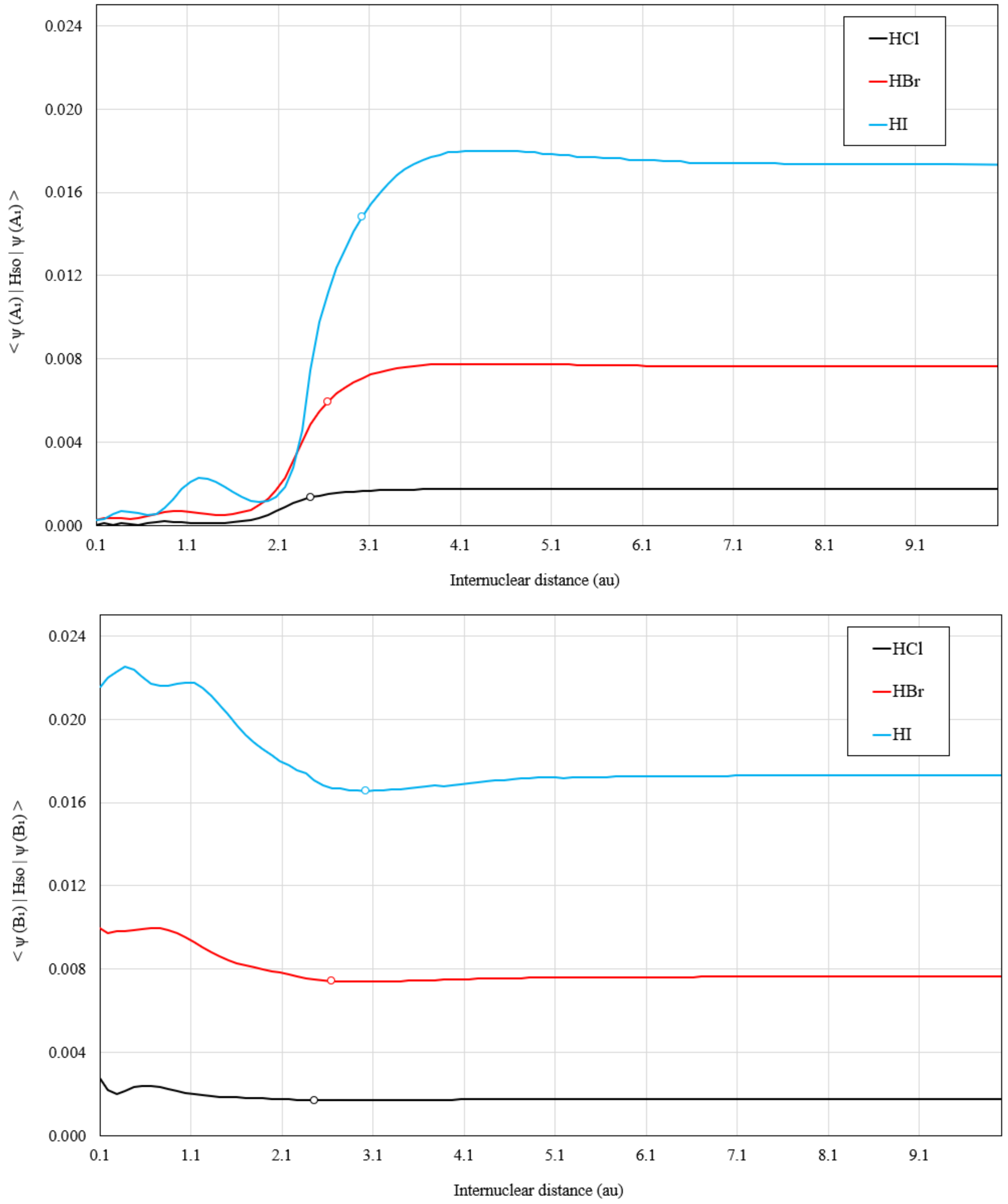

Figure 8: Spin-orbit (SO) couplings modules between states of A_1 (top panel) and B_1 (bottom panel) irreps. in HCl, HBr and HI. SO coupling effects have been calculated in spin-free symmetry adapted basis. Empty points indicate the molecule equilibrium distance.

4.3 Quantum wave packet propagation

4.3.1 Laser description

In the present work, we are investigating the dynamics in the time scale of a few femtoseconds (2-14 fs), which is too short to allow for molecular rotation[55;57]. Light pulses with low intensities are considered, such that non-linear processes can be disregarded; laser intensity is 10^{12} W cm^{-2}, that corresponds to a field maximum amplitude $E_0 = 5.33761 \cdot 10^{-3}$ au.

Total pulse duration is fixed in T= 2 fs (82.6788 au) and it is defined with a sine-squared envelope function F(t). Light polarization vectors perpendicular (E_x and E_y) and parallel (E_z) to molecular axis are employed. Electric field is numerically described in equation 59.

$$\text{E(t)} \begin{cases} E(t) = 0.00533761 \cdot cos^2\left(\frac{\pi}{82.6788} \cdot t\right) \cdot cos\left(\omega t\right) & t = [0, 2 \text{ fs}] \\ 0 & \text{t = elsewhere} \end{cases} \tag{59}$$

Since both x and y-directions are equivalents in C_{2v} point group with respect to the bond axis (z-axis), wave packet propagation is shown only for the x-direction (identical results are obtained along the y-axis). In order to carry out a meaningful comparison between the three molecules, different central pulse frequencies are employed for each molecule.

Central frequency of the pulse is chosen to be resonant with the transition to the first excited state ($^1\Pi$ in spin-free, 1Π in adiabatic). The heavier the halogen, the closer in energy are the eigenvalues; therefore, the resonant excitation occurs at lower frequencies. Specifically, we will use the excitation frequencies in a vertical transition from the equilibrium distance, i.e. 7.10 eV (0.261 au) for HCl, 6.05 eV (0.222 au) for HBr and 5.08 eV (0.187 au) for HI. Total duration and laser intensity are kept constant.

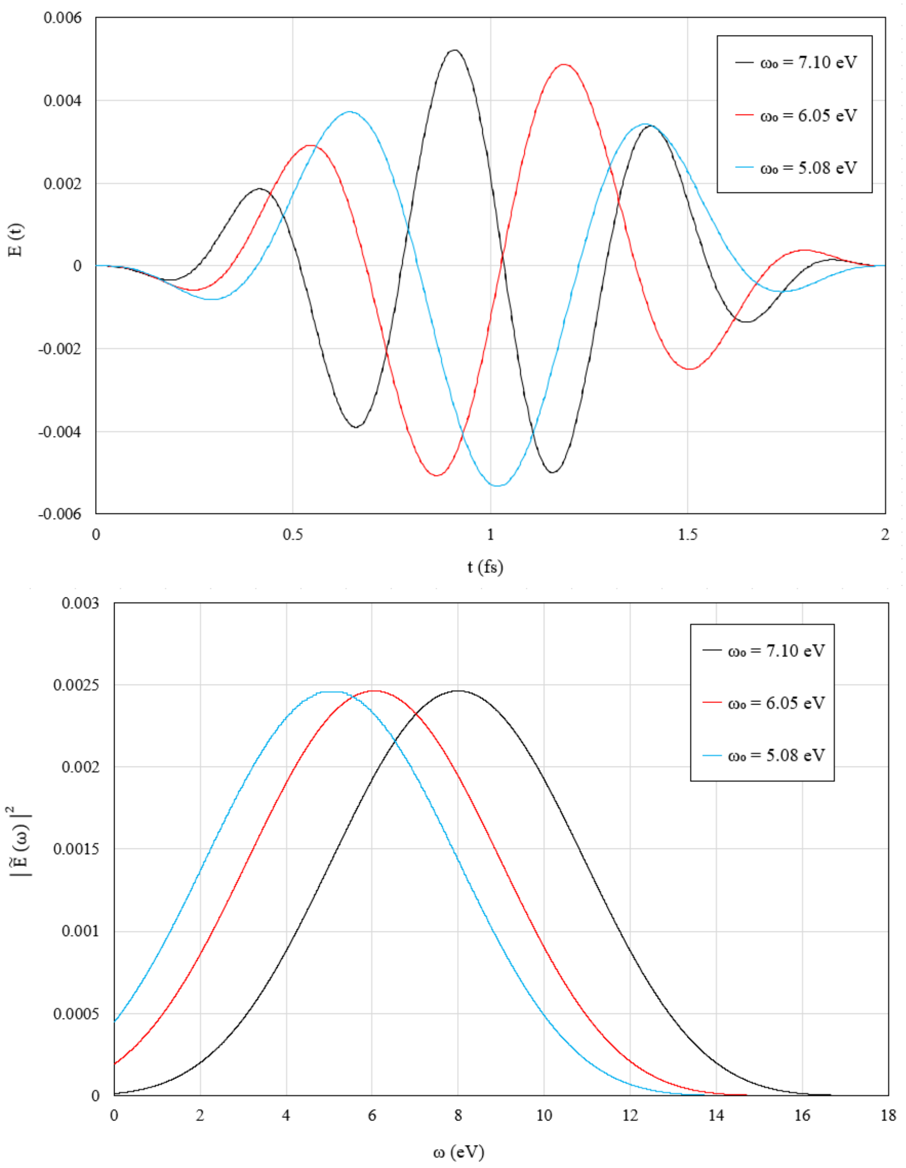

Figure 9: Electric field as a function of time (left side panel) and frequency (right side panel) for the three pulses employed for the three molecules. Central frequencies are chosen to be resonant with the vertical transition to the first excited state ($^1\Pi$ working in spin-free, 1Π working in adiabatic). Total duration and laser intensities are fixed at 2 fs and $10^{12} W/cm^2$.

Figure 9 shows the ultrashort pulses employed to excite the molecules as a function of time (left panel) and as a function of energy (right panel). Different central frequencies are used depending on the molecule, which is clearly shown in the energy distribution of the pulses shown on the right side panel: maximum of the field amplitude Fourier transform $|\tilde{E}(\omega)|^2$ is at the photon energy difference between $1\Sigma^+$ and 1Π in order to obtain the highest possible excitation probability.

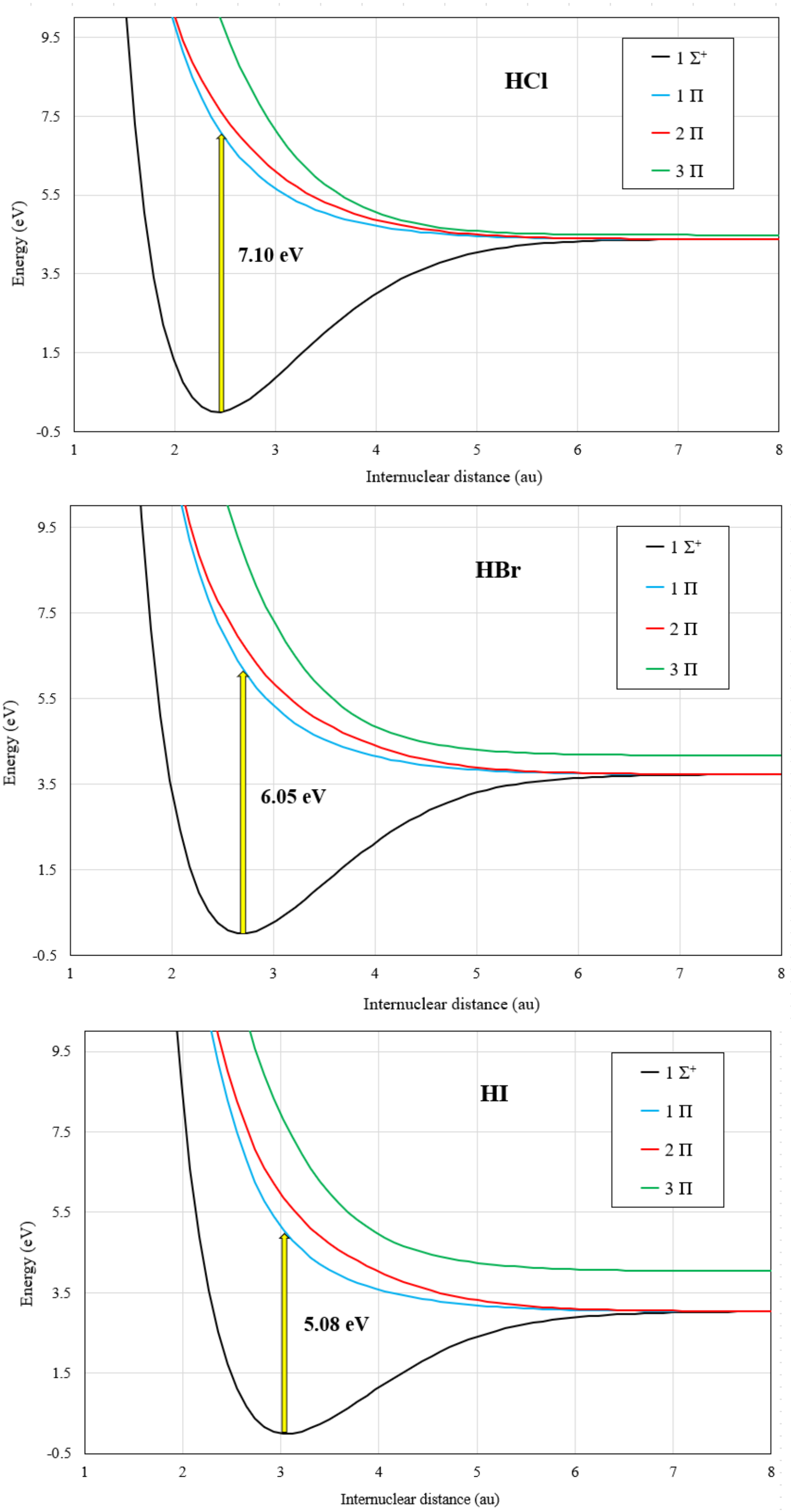

Figure 10: Potential energy curves of the three hydrogen halides with respect to their ground states. The four states are those involve in the dynamics of excitation with x-polarized light. Energy difference shown in arrow is the photon energy used for the laser pulse.

4.3.2 TDSE solution: wave packet propagation

Once spin-free symmetry adapted and adiabatic potential energy curves, dipole and spin-orbit couplings between vibronic states and the laser pulse features are known, the next step is to solve the time-dependent Schrödinger equation, to obtain the time evolution of coefficients $c_j(t)$, i.e. the combination of the basis functions that represents the wave packet $\Psi(t)$. TDSE is solved in the interaction picture in the length gauge using Runge-Kutta integration method.

$$\Psi(t) = \sum_j c_j(t)\, |\psi_j\rangle$$

$$i\,\frac{\partial \mathbb{C}(t)}{\partial t} = \left[\hat{\mathbb{T}}_N + \hat{\mathbb{V}}_{el} - \Lambda + \hat{\mathbb{H}}_{SO} + \bar{\mu} \cdot \hat{\mathbb{E}}(t)\right]\, \mathbb{C}(t)$$

Time propagation is performed for times up to 14 fs; at $t = 14$ fs the nuclear wave packet distributions reach internuclear distances around 10 au, i.e. for longer times the nuclei will reach distances around the radial box edge ($R_{max} = 13$ au) in which vibrational Schrödinger equation has been solved, and nonphysical reflections will show up.

Figure 11 shows the wave packets propagation over **spin-free (SF)** states for the three molecules, meaning spin-orbit coupling is not included. The dynamics follows the same trend in the three molecules: due to the presence of a dipole coupling μ_x between $^1\Sigma^+$ and $^1\Pi$ states, x-polarized laser causes transfers population from ground state to excited state and double-degenerated $^1\Pi$ electronic state is populated. Due to moment distribution occurs only in this state, at the end of the propagation the spin-free wave packets achieves only the dissociation channel $H(^2S) + X(^2P)$.

At the end of the pulse ($t = T = 2$ fs), the excited state $^1\Pi$ is populated and the density of excitation probability in all the molecules is still located close to the molecular equilibrium distance, as it is observed in black line of figure 11). Nuclear wave packets are located around 2.43, 2.74 and 2.87 au in HCl ($R_{eq} = 2.41$ au), HBr ($R_{eq} = 2.67$ au) and HI ($R_{eq} = 3.04$ au), respectively. This means that at the beginning, the molecule has been excited but the nuclei had not too much time to move away from the initial distance given by the equilibrium geometry of the ground state.

After the pulse ends ($t > 2$ fs), wave packets evolve towards larger internuclear distances. With the evolution in time, the wave packets distributions are wider in the range of internuclear distances, meaning the probability distributes over a larger range of nuclear geometries. Working in spin-free states, since the nuclear wave packet moves over the purely dissociative state $^1\Pi$ in all the halides, with the evolution the nuclei accumulate momentum and it keeps moving forward, i.e. **it keeps dissociating**.

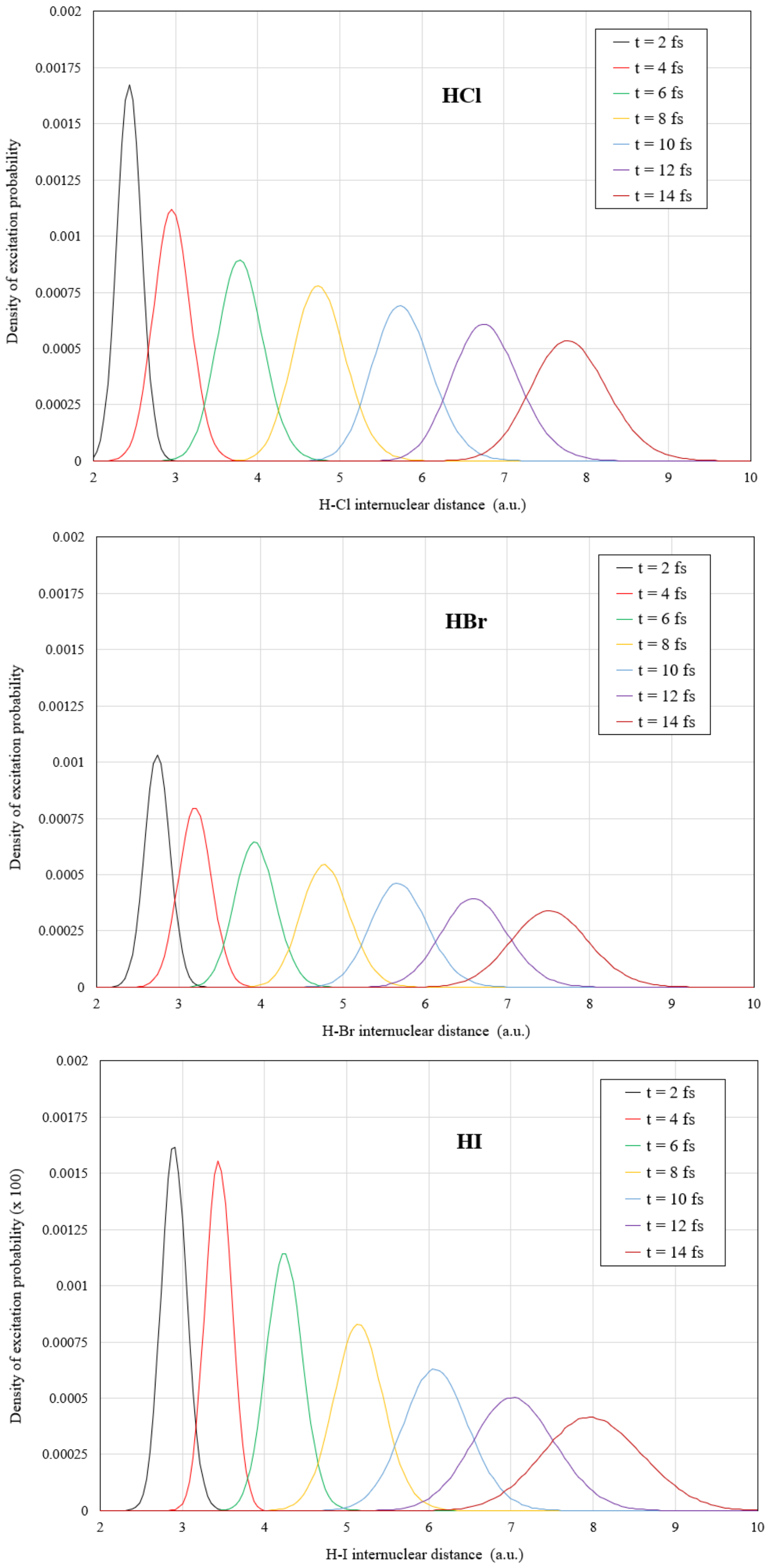

Figure 11: In diabatic picture (spin-free Hamiltonian), $^1\Pi$ state wave packet evolution of the three hydrogen halides. Excitation from ground state has been done with a x-polarized laser pulse.

Comparing the three hydrogen halides propagation in spin-free, the highest excitation probability occurs in HCl and the lowest in HI. This occurs because, although the maximum dipole coupling between $^1\Sigma^+$ and $^1\Pi$ states has the highest value in HI, the relevant values are those in the Franck-Condon region, meaning those in the range covered by the ground state. As it can be noticed in figure 6, transition dipole moment at the equilibrium distance values around 0.22, 0.19 and 0.05 au for HCl, HBr and HI, respectively. This is the reason why our one-photon excitation probabilities follow this trend.

The goal of this work is to explore the relevance of the **spin-orbit couplings** in hydrogen halides molecular dissociation. Therefore, working with spin-free symmetry adapted (SA) representation, spin-orbit operator is included in the Hamiltonian, what allows the coupling of electronic states with the same symmetry. Figure 12 shows the wave packets in the three SA states belonging to B_1 irrep at four different times: 2, 6, 10 and 14 fs. The same laser has been used for both spin-free and adiabatic simulations, i.e. at each evolution time the sum of the three SA states (1Π,2Π,3Π) wave packets probabilities gives the same probability that SF ($^1\Pi$) wave packet:

$$|\Psi_{^1\Pi}^{SF}\ (R,t)|^2 = |\Psi_{1\Pi}^{SA}\ (R,t)|^2 + |\Psi_{2\Pi}^{SA}\ (R,t)|^2 + |\Psi_{3\Pi}^{SA}\ (R,t)|^2$$

In the first place, in **HCl**, when the laser pulse ends ($t = 2$ fs) the only wave packet with significant probability is the 1Π adiabatic state, i.e. there has only been population transfer from ground state $1\Sigma^+$ to excited state 1Π. Over the evolution of the wave packet, the excitation probability of 1Π state decreases while 2Π and 3Π probability increases. This means that there have been population transfer to 2Π and 3Π states, i.e. population transfer between B_1 states along the potential curve occurs due to the presence of previously explained spin-orbit couplings $\langle B_1|\ \hat{H}^{SO}\ |B_1\ \rangle$, observed in fig. 8.

At the end of the HCl propagation ($t = 14$ fs), 1Π state is the one with largest probability and it is remarkable that excitation probability is higher in 2Π state than 3Π. Due to SO coupling with 1Π state values the same for both states at equilibrium distance, this probability difference must occur because the presence of a higher energy gap between 1Π and 3Π, as it can be noticed in their energy curves (fig. 1). At larger distances the highest populated states 1Π and 2Π lead to dissociation channel $H(^2S)+X(^2P_{\frac{3}{2}})$, while the dissociation via $H(^2S) + X^*(^2P_{\frac{1}{2}})$ in 3Π wave packet has less density of probability.

In the second place, in **HBr**, just when the pulse ends ($t = 2$ fs) it is observed not only 1Π wave packet, but also the 3Π state is populated, and the maximums are placed at the same internuclear distance. As wave packets evolve, there is population transfer between the three B_1 states and it is observed difference in the wave packets velocities: at $t = 6$ fs, maximums of 1Π and 3Π are at the same internuclear distance but 2Π state maximum is placed at larger distances. At $t = 14$ fs, state 1Π is at the longest distance, state 2Π is at the shortest distance and state 3Π is in the middle of the previous ones. In fact, at the end of the propagation the 2Π wave packet is the one with the highest excitation probability. This occurs because spin-orbit coupling between B_1 states is much larger in HBr than in HCl.

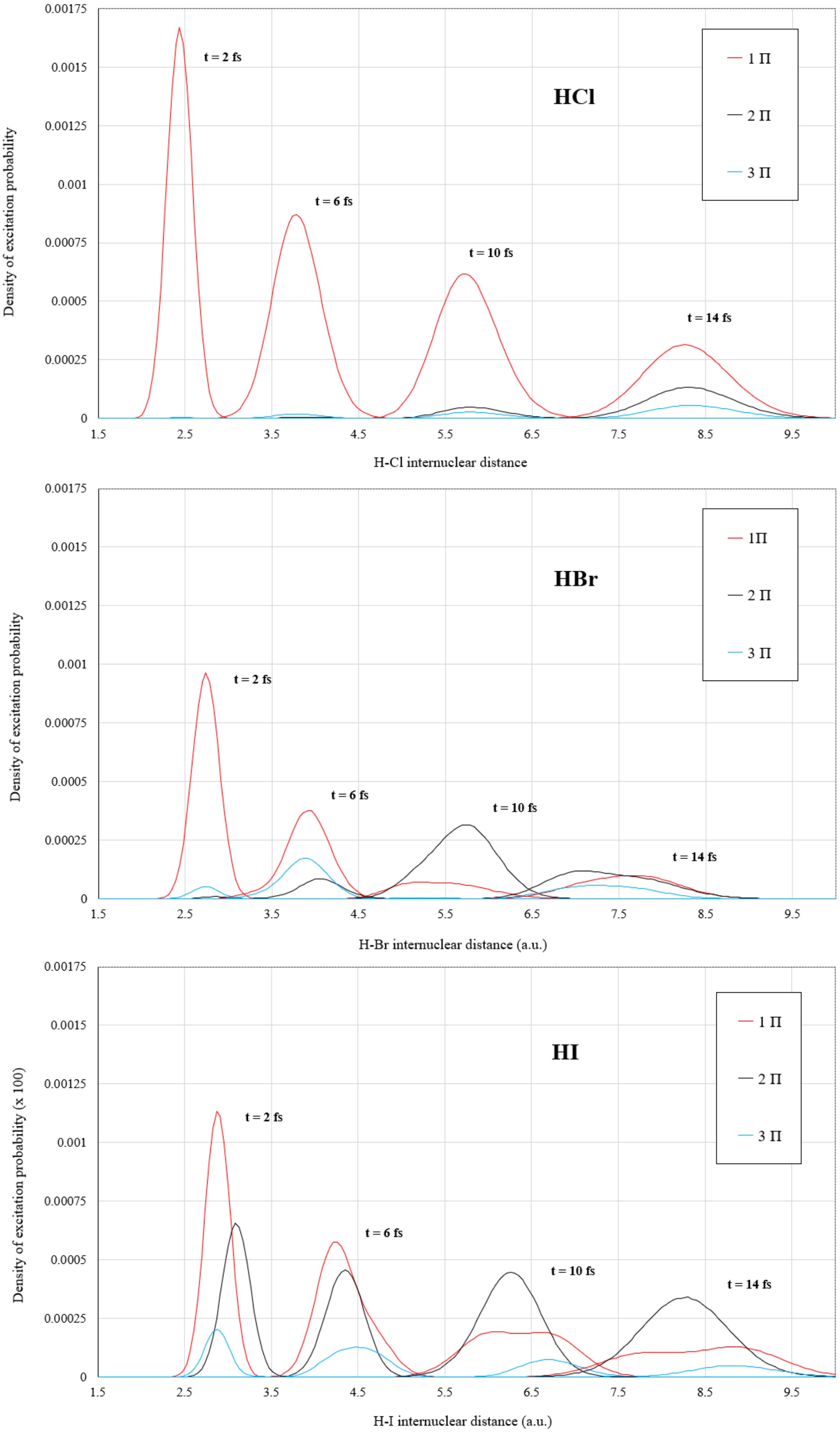

Figure 12: In adiabatic picture (including spin-orbit Hamiltonian), wave packet evolution of the three symmetry B_1 states (1Π, 2Π and 3Π) of the three hydrogen halides. Excitation from ground state has been done with a x-polarized laser pulse.

In the third place, wave packet equilibrium distance changes are even more remarkable in the case of **HI**. At the beginning of the propagation $t = 2$ fs, total probability is distributed over the three states: 1Π is the highest populated state but there is significant population transfer to 2Π and 3Π states, much more than in HCl and HBr because spin-orbit coupling is much higher in HI. Due to potential energy curves of the three states have different gradients (fig. 3), the nuclei accumulate momentum differently: 1Π and 3Π states have parallel gradients, they have the same velocity and for this reason they are centered at the same distance, but 2Π gradient is much greater, it accumulates momentum at higher velocity (more momentum and more energy in less time) and it is centered at a longer distance.

At $t = 6$ fs, nuclear wave packets are centered at different distances (3Π and 1Π at largest and shortest distance, respectively) and are distributed over a range of internuclear distances between 3.5 and 5 au. As HI potential energy curves shown, at these distances the three states have crossed and present a strong coupling, observed in their strong energy splitting.

At $t = 10$ fs, two different peaks can be perfectly distinguished in 1Π state (red line), meaning now there are two components with different accumulate momentum in this wave packet. As in shorter times, each nuclear wave packet accumulates momentum differently following its potential energy curve with its own velocity. The second peak, due to it is situated over the distance at which 3Π maximum is placed (6.8 au), indicates that there has been **"back" population transfer from 3Π to 1Π**. For this reason the same red wave packet begins to have two peaks, what means different momenta as the population goes from into the 1Π state.

This two-peak structure of 1Π wave packet is clearer observed looking at the excitation probabilities at 14 fs: two well defined peaks are observed at 7.6 and 8.7 au, and again the second peak is centered at the same distance that 3Π. Moreover, on both 10 and 14 fs, population transfer from 3Π to 1Π makes that the wave packet that belongs to 2Π state becomes the one with highest density of excitation probability (black line).

As a conclusion, it can be deduced that shape and velocity differences between the wave packets mainly occurs due to three facts:

- The **spin-orbit coupling variation**: there is more population transfer between B_1 states where spin-orbit coupling variation is higher, meaning when the gradient of figure 8 graphs is higher. This gradient values 0.018 in HI, 0.008 in HBr and 0.002 in HCl.
- The **energy gap between coupled electronic states**: energy difference between both electronic states is lower when the hydrogen halide mass increases, and the closer the curves are, the more population transfer there can be. This is related with spin-orbit coupling, because there is a larger value of spin-orbit coupling where there is less energy difference between electronic states.
- The **energy gradient in the potential energy curve**: the more the gradient in potential energy curve, the higher is the velocity of the wave packet, i.e. the momentum accumulation with respect to the time.

4.3.3 TDSE solution: Probability Evolution

Excited states can be better understood not only by observing wave packets evolution, but also by plotting the density of excitation probability $|\Psi(t)|^2$ working in SA basis $|\psi_j^{SA}\rangle$ versus the vibrational energy of the excited vibronic state. This is shown in figure 13 at different integration times in the three molecules. On left panels, it is plotted the excitation probabilities of 1Π state and the probability working in SF basis just at the end of the pulse ($t = 2$ fs). In spin-free system, only degenerated $^1\Pi$ electronic state is populated and there is no population transfer to other states. On right side panels, excitation probabilities of 2Π and 3Π states are observed.

In the first place, the above two plots in fig. 13 correspond to excitation probabilities of the three B_1 states in **HCl**. At the end of the pulse ($t = 2$ fs), there has been population transfer only from ground state $^1\Sigma^+$ to excited state 1Π, but not to other same-symmetry state has been plotted, i.e. wave packet is basically the same as the one in spin-free $^1\Pi$ state.

As time increases, wave packet moves over with a certain velocity, $^1\Pi$ density of probability decreases while 2Π and 3Π excitation probabilities increases; there has been population transfer due to the presence of SO coupling $\hat{H}^{SO}$. 2Π state (dissociation channel $H(^2S)+X(^2P_{\frac{3}{2}})$) increases its population more than 3Π (dissociation channel $H(^2S) + X^*(^2P_{\frac{1}{2}})$) does. In fact, there is only a slight change in the excitation probabilities, i.e. there exists population transfer from the 1Π to 2Π and 3Π, but there is no population come back to 1Π state.

In the second place, the middle two panels, corresponding to excitation probabilities of B_1 states in **HBr**, differ with those in HCl. 1Π wave packet (blue plot on the left middle picture) has less probability than SF wave packet because excited state 3Π is populated too. In 1Π plots (left panel), from 2 to 10 fs, the probability maximum not only decreases, but also it shifts to lower energies. On 2Π and 3Π state (right side panels), from 2 to 10 fs the probability maximum increases and it shifts to higher energies, i.e. although population transfer occurs, the **energy of the total wave packet** (sum of 1Π, 2Π and 3Π) **is constant** during evolution. At $t = 14$ fs, 1Π states maximum increases and it shifts again to the right while 2Π and 3Π maximum decreases and it shifts to the left.

In the third place, **HI** molecule plots (bottom of fig. 13) show a remarkable feature: at the end of the pulse ($t = 2$ fs), there is a smooth single-peak distribution for the 1Π state (blue line in left panel), and these smooth excitation probabilities are also observed in 2Π and 3Π states (dashed and full blue lines in the right side panel). This is clearly observed in HI due to the spin-orbit coupling between 1Π state and 2Π and 3Π states is much larger for HI than for HCl and HBr.

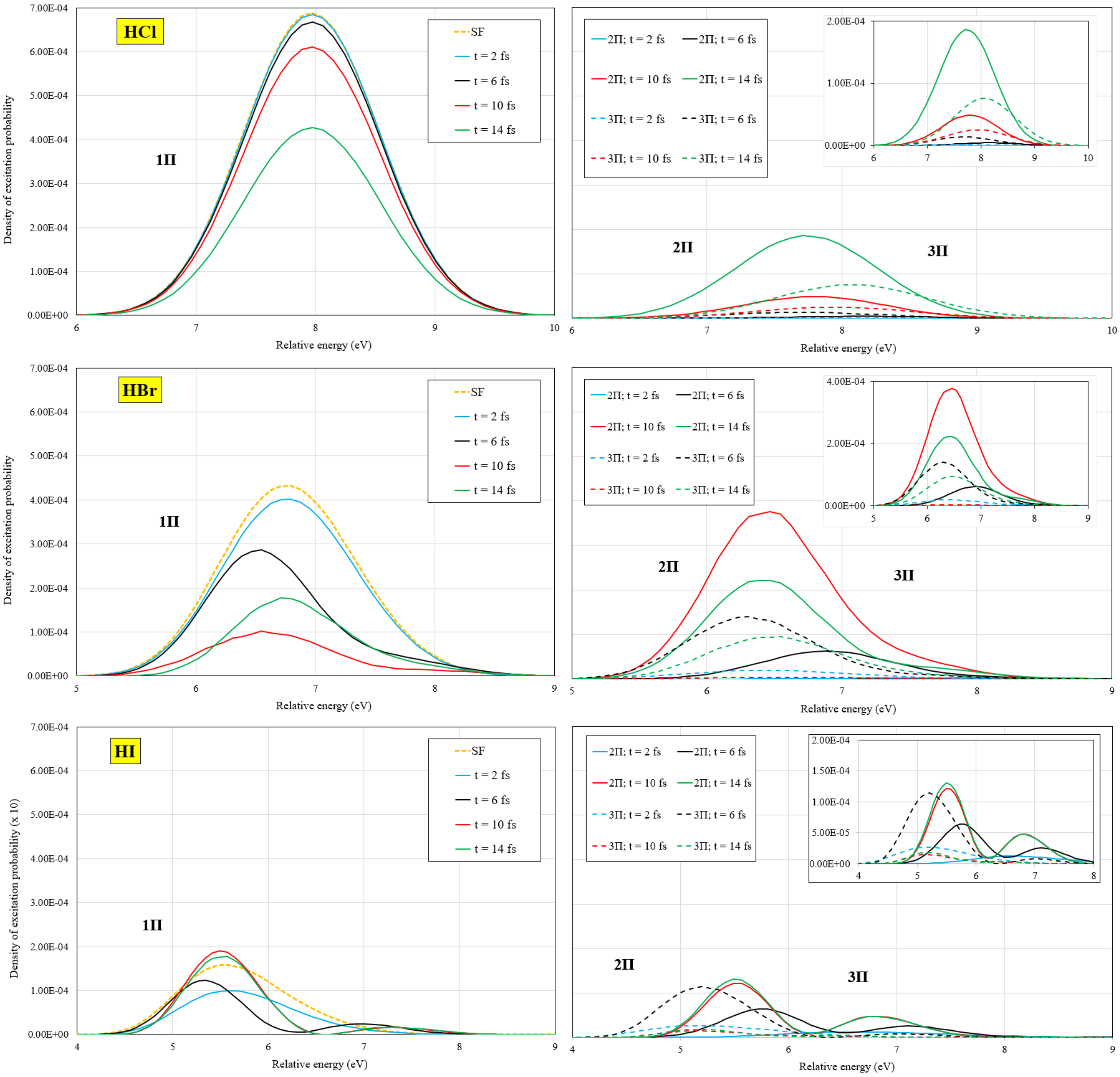

Figure 13: Density of excitation probability of the three B_1 states (1Π, 2Π and 3Π) at different times versus excited vibrational state energies. Wave packets have been obtained using x-polarized laser pulse, perpendicular to the molecular axis. Spin-free wave packet obtained at 2 fs is also plotted.

At $t = 2$ fs the three electronic states have crossed, nuclear wave packets are distributed over 3.5-5.0 au and they present a strong coupling, i.e. a strong energy splitting. Because these potential energy curves have a different gradient, nuclei accumulate momentum differently and it is possible to distinguish two well different peaks as the population goes into the 1Π state. At larger times such as 10 or 14 fs, this two peaks are perfectly well-defined around 5.5 the first and 7.5 eV the second one.

Two-peaked structure is observed when states involved in spin-orbit coupling have different gradient in potential energy curves. Therefore they have different momentum accumulation with respect to the time, what is reflected in maximum shifted to different energies. Although population transfer back is more noticeable in HI, these effects are gradually observed in the HCl and HBr. In HCl, SO coupling has the lowest value and there is the highest difference between B_1 states at equilibrium distance; for this reason no momentum transference is observed between 2 and 14 fs. In HBr, SO coupling increases and the energy separation between states decreases, meaning there is a larger energy splitting and it is noticed population transfer.

This is the reason why in fig. 13, as an example, 1Π probability at 6 fs in HCl (black line in fist left panel) shows a perfectly Gaussian distribution over the energies range, in HBr (black line in second left panel) it is observed a smooth "band" on the right and in HI (black line in third left panel) two different peaks are perfectly noticed. In fact, if the propagation in HCl or HBr was carried out for a longer time and in a larger box, there would exist stronger energy coupling, i.e. a peak in the wave packets shape would appear.

5 Conclusions and Future Perspectives

We have implemented a procedure for a time-dependent treatment of molecular dissociation induced by ultrashort laser pulses, in order to investigate the ultrafast molecular dynamics in hydrogen halides photodissociation process and, specifically, the effect of accounting for spin-orbit couplings in this dynamics, a non-adiabatic effect. We accurately compute the excitation probabilities using different laser parameters for three hydrogen halides: HCl, HBr and HI. We examine the effect of the non-adiabatic couplings in real time, tracking the evolution of coupled electron-nuclear dynamics triggered upon excitation with an ultrashort pulse.

In this study, two different approaches have been employed: firstly, a spin-free representation of the molecular states, where the spin-orbit couplings are ignored, and, secondly, a simulation in the adiabatic picture properly accounting for the spin-orbit effects. Calculations are thus performed by using spin-free states Ψ^{SF}, defined by their angular momentum Λ and their spin S, and by expanding the spin-orbit states into spin-free symmetry adapted basis, defined by their angular momentum Λ, spin S and spin projection M_S, i.e. spin-orbit states are defined as lineal combination of spin-free states.

The time-dependent molecular wave function is calculated quantum mechanically in full dimensionality, by numerically solving the time-dependent Schrödinger equation. We use a spectral method, where the time-dependent wave function is expanded in a set of molecular eigenstates, which are computed within the Born-Huang approximation. Firstly, the Quantum Chemistry package MOLPRO has been used to obtain the electronic structure at different nuclear configurations of the molecules working with a MRCI method and employing ANO-RCC basis sets. Vibrational wave functions are then calculated by expanding the nuclear wave functions in a B-spline basis sets, which provides an accurate representation of the vibrational continuum states associated to the purely dissociative electronic excited states of the molecules. Then, dipole couplings of spin-free states and dipole and spin-orbit couplings of adiabatic states are calculated. Afterwards, time-dependent Schrödinger equation is solved at different times, obtaining a time-resolved picture of the photo-dissociation process. The three molecules are excited by using different ultrashort laser pulses in the order of fs, time scale in which spin-orbit effects are observed. It has been provide a **full description to explore the excitation dynamics of hydrogen halides**.

The work presented is part of an ongoing project; the next step involves the projection into the adiabatic states to retrieve the relative ratios of the fragmentation channels, which could be directly compared with an eventual UV-induced excitation experiment on these targets. The computational tools to perform this projection (obtaining the rotation matrix) have been also developed, as well as the necessary codes to retrieve fragmentation ratios. Further investigation of the possibility of manipulating the excitation dynamics by tailoring the UV pulses is already in progress, since the numerical tools have been fully developed for the present study.

References

[1] Roadmap on dynamics of molecules and clusters in the gas phase. H. Zettergren et al., The European Physical Journal D 75, 1-53 (2021)

[2] Sullivan, J. M., & Shukla, P. (1999). Time-resolved rhodopsin activation currents in a unicellular expression system. Biophysical journal, 77(3), 1333-1357.

[3] Agostini, F., & Curchod, B. F. (2019). Different flavors of nonadiabatic molecular dynamics. Wiley interdisciplinary reviews: computational molecular science, 9(5), e1417.

[4] Jasper, A. W., Zhu, C., Nangia, S., & Truhlar, D. G. (2004). Introductory lecture: Nonadiabatic effects in chemical dynamics. Faraday Discussions, 127, 1-22.

[5] H. Yoshinaga et al., RSC Advances, 6, 65020-65030 (2016)

[6] Péoux, G., Monnerville, M., Duhoo, T., & Pouilly, B. (1997). Spin–orbit branching in the photodissociation of HBr: Time-independent, time-dependent, and semiclassical calculations. The Journal of chemical physics, 107(1), 70-82.

[7] Alexander, M. H., Pouilly, B., & Duhoo, T. (1993). Spin–orbit branching in the photofragmentation of HCl. The Journal of chemical physics, 99(3), 1752-1764.

[8] Magnotta, F., Nesbitt, D. J., & Leone, S. R. (1981). Excimer laser photolysis studies of translational-to-vibrational energy transfer. Chemical Physics Letters, 83(1), 21-25.

[9] Franco de Carvalho, F., & Tavernelli, I. (2015). Nonadiabatic dynamics with intersystem crossings: A time-dependent density functional theory implementation. The Journal of chemical physics, 143(22), 224105.

[10] Guenin, M. (1966). On the interaction picture. Communications in Mathematical Physics, 3(2), 120-132.

[11] Bhatti, M. I., & Debnath, L. (2004). On fractional Schrodinger and Dirac equations. International Journal of Pure and Applied Mathematics, 15, 1-12.

[12] Born, M., & Fock, V. (1928). Beweis des adiabatensatzes. Zeitschrift für Physik, 51(3-4), 165-180.

[13] Kerley, G. I. (2013). On Corrections to the Born-Oppenheimer Approximation. arXiv preprint arXiv:1306.6574.

[14] Atkins, P. W., & Friedman, R. S. (2011). Molecular quantum mechanics. Oxford university press. Page 40.

[15] Worth, G. A., Robb, M. A., & Lasorne, B. (2008). Solving the time-dependent Schrödinger equation for nuclear motion in one step: direct dynamics of non-adiabatic systems. Molecular Physics, 106(16-18), 2077-2091.

[16] Reimers, J. R., McKemmish, L. K., McKenzie, R. H., & Hush, N. S. (2015). Non-adiabatic effects in thermochemistry, spectroscopy and kinetics: the general importance of all three Born–Oppenheimer breakdown corrections. Physical Chemistry Chemical Physics, 17(38), 24641-24665.

[17] Worth, G. A., & Cederbaum, L. S. (2004). Beyond Born-Oppenheimer: molecular dynamics through a conical intersection. Annu. Rev. Phys. Chem., 55, 127-158.

[18] M. Born and K. Huang, Dynamical Theory of Crystal Lattices, Clarendon, Oxford, (1954)

[19] Atkins, P. W., & Friedman, R. S. (2011). Molecular quantum mechanics. Oxford university press. Page 250.

[20] Jensen, F. (2017). Introduction to computational chemistry. John wiley & sons. Pages 138-142.

[21] Jensen, F. (2017). Introduction to computational chemistry. John wiley & sons. Pages 158-160.

[22] Martín, F. (1999). Ionization and dissociation using B-splines: photoionization of the hydrogen molecule. Journal of Physics B: Atomic, Molecular and Optical Physics, 32(16), R197.

[23] Simeonov, P., & Goldman, R. (2013). Quantum B-splines. BIT Numerical Mathematics, 53(1), 193-223.

[24] H. Bachau, E. Cormier, P. Decleva, J. E. Hansen and F. Martín, "Applications of B-Splines in Atomic and Molecular Physics," Reports on Progress in Physics, Vol. 64, No. 12, 2001, p. 1815. doi:10.1088/00344885/64/12/205.

[25] Yarkony, D. R. (1992). Spin-forbidden chemistry within the Breit-Pauli approximation. International Reviews in Physical Chemistry, 11(2), 195-242.

[26] Pitzer, K. S. (1979). Relativistic effects on chemical properties. Accounts of Chemical Research, 12(8), 271-276.

[27] Dirac, P. A. M. (1928). The quantum theory of the electron. Proceedings of the Royal Society of London. Series A, Containing Papers of a Mathematical and Physical Character, 117(778), 610-624.

[28] Bade, W. L., & Jehle, H. (1953). An introduction to spinors. Reviews of Modern Physics, 25(3), 714.

[29] Mussard, B., & Sharma, S. (2018). One-step treatment of spin–orbit coupling and electron correlation in large active spaces. Journal of chemical theory and computation, 14(1), 154-165.

[30] Pauli, W. (1988). Zur quantenmechanik des magnetischen elektrons. In Wolfgang Pauli (pp. 282-305). Vieweg+ Teubner Verlag.

[31] Carreras, A., Jiang, H., Pokhilko, P., Krylov, A. I., Zimmerman, P. M., & Casanova, D. (2020). Calculation of spin–orbit couplings using RASCI spin-less one-particle density matrices: Theory and applications. The Journal of Chemical Physics, 153(21), 214107.

[32] Nakajima, T., & Hirao, K. (2012). The Douglas–Kroll–Hess Approach. Chemical reviews, 112(1), 385-402.

[33] Sucher, J. (1980). Foundations of the relativistic theory of many-electron atoms. Physical Review A, 22(2), 348.

[34] Dyall, K. G., & Fægri Jr, K. (2007). Introduction to relativistic quantum chemistry. Oxford University Press.

[35] Bauschlicher, C. W., & Partridge, H. (1993). On the invariance of the configuration interaction energy with respect to orbital rotations. Theoretica chimica acta, 85(4), 255-259.

[36] Meitei, O. R., Houck, S. E., & Mayhall, N. J. (2020). Spin–orbit matrix elements for a combined spin-flip and IP/EA approach. Journal of chemical theory and computation, 16(6), 3597-3606.

[37] Atkins, P. W., & Friedman, R. S. (2011). Molecular quantum mechanics. Oxford university press. Pages 543-546.

[38] Draine, B. T. (1988). The discrete-dipole approximation and its application to interstellar graphite grains. The Astrophysical Journal, 333, 848-872.

[39] Boßmann, L. (2016). On the Dipole Approximation (Doctoral dissertation, Master Thesis).

[40] Forre, M., & Simonsen, A. S. (2016). Generalized velocity-gauge form of the light-matter interaction Hamiltonian beyond the dipole approximation. Physical Review A, 93(1), 013423.

[41] Palacios, A., Horner, D. A., Rescigno, T. N., & McCurdy, C. W. (2010). Two-photon double ionization of the helium atom by ultrashort pulses. Journal of Physics B: Atomic, Molecular and Optical Physics, 43(19), 194003.

[42] González-Castrillo, A., Pérez-Torres, J. F., Palacios, A., & Martín, F. (2011). Probing vibrational wave packets in molecular excited states. Theoretical Chemistry Accounts, 128(4), 735-742.

[43] Kasdin, N. J. (1995). Runge-Kutta algorithm for the numerical integration of stochastic differential equations. Journal of Guidance, Control, and Dynamics, 18(1), 114-120.

[44] Werner, H. J., Knowles, P. J., Knizia, G., Manby, F. R., Schutz, M., & Celani, P. (2010). Molpro.

[45] Bibtex entry: @MiscDIRAC21, note = "DIRAC, a relativistic ab initio electronic structure program, Release DIRAC21 (2021), written by R. Bast, A. S. P. Gomes, T. Saue, L. Visscher, and H. J. Aa. Jensen, with contributions from I. A. Aucar, V. Bakken, K. G. Dyall, S. Dubillard, U. Ekström, E. Eliav, T. Enevoldsen, E. Faßhauer, T. Fleig, O. Fossgaard, L. Halbert, E. D. Hedegård, T. Helgaker, B. Helmich–Paris, J. Henriksson, M. Iliaš, Ch. R. Jacob, S. Knecht, S. Komorovský, O. Kullie, J. K. Lærdahl, C. V. Larsen, Y. S. Lee, N. H. List, H. S. Nataraj, M. K. Nayak, P. Norman, G. Olejniczak, J. Olsen, J. M. H. Olsen, A. Papadopoulos, Y. C. Park, J. K. Pedersen, M. Pernpointner, J. V. Pototschnig, R. di Remigio, M. Repisky, K. Ruud, P. Sałek, B. Schimmelpfennig, B. Senjean, A. Shee, J. Sikkema, A. Sunaga, A. J. Thorvaldsen, J. Thyssen, J. van Stralen, M. L. Vidal, S. Villaume, O. Visser, T. Winther, and S. Yamamoto (available at `http://dx.doi.org/10.5281/zenodo.3572669`, see also `http://www.diracprogram.org`)"

[46] Roos, B. O., Lindh, R., Malmqvist, P. Å., Veryazov, V., & Widmark, P. O. (2004). Main group atoms and dimers studied with a new relativistic ANO basis set. The Journal of Physical Chemistry A, 108(15), 2851-2858.

[47] Regan, P. M., Ascenzi, D., Brown, A., Balint-Kurti, G. G., & Orr-Ewing, A. J. (2000). Ultraviolet photo-dissociation of HCl in selected rovibrational states: Experiment and theory. The Journal of Chemical Physics, 112(23), 10259-10268.

[48] Smolin, A. G., Vasyutinskii, O. S., Balint-Kurti, G. G., & Brown, A. (2006). photo-dissociation of HBr. 1. Electronic structure, photo-dissociation dynamics, and vector correlation coefficients. The Journal of Physical Chemistry A, 110(16), 5371-5378.

[49] Wang, F., Lu, I. C., Yuan, K., Cheng, Y., Wu, M., Parker, D. H., & Yang, X. (2007). photo-dissociation dynamics of HI and DI at 157 nm. Chemical Physics Letters, 449(1-3), 18-22.

[50] Huber, K.P.; Herzberg, G., Molecular Spectra and Molecular Structure. IV. Constants of Diatomic Molecules, Van Nostrand Reinhold Co., 1979.

[51] Radziemski, L. J., & Kaufman, V. (1969). Wavelengths, energy levels, and analysis of neutral atomic chlorine (Cl I). JOSA, 59(4), 424-443.

[52] Davies, P. B., Thrush, B. A., Stone, A. J., & Wayne, F. D. (1972). The gas-phase electron paramagnetic resonance spectrum of excited (4p52P12) bromine atoms. Chemical Physics Letters, 17(1), 19-21.

[53] Luc-Koenig, E., Morillon, C., & Verges, J. (1975). Etude Expérimentale et Théorique de l'Iode Atomique. Observation du Spectre d'Arc Infrarouge, Classification et Structure Hyperfine. Physica Scripta, 12(4), 199.

[54] NIST Computational Chemistry Comparison and Benchmark Database. NIST Standard Reference Database Number 101. Release 21, August 2020, Editor: Russell D. Johnson III. http://cccbdb.nist.gov/. DOI:10.18434/T47C7Z

[55] Valero, R., Truhlar, D. G., & Jasper, A. W. (2008). Adiabatic states derived from a spin-coupled diabatic transformation: Semiclassical trajectory study of photo-dissociation of hbr and the construction of potential curves for libr+. The Journal of Physical Chemistry A, 112(25), 5756-5769.

[56] Werner, H. J., & Rosmus, P. (1980). Theoretical dipole moment functions of the HF, HCl, and HBr molecules. The Journal of Chemical Physics, 73(5), 2319-2328.

[57] Givertz, S. C., & Balint-Kurti, G. G. (1986). Prediction of the Cl (2 P 3/2)/Cl (2 P 1/2) branching ratio in the photo-dissociation of HCl. Journal of the Chemical Society, Faraday Transactions 2: Molecular and Chemical Physics, 82(8), 1231-1242.

[58] Palacios, A., González-Castrillo, A., Bachau, H., & Martín, F. (2014, April). Wave packet dynamics in molecular excited electronic states. In Journal of Physics: Conference Series (Vol. 488, No. 1, p. 012017).